Norwegian University of Science and Technology
NTNU

Department of Chemical Engineering

Associate Prof. Johannes Jäschke

Modeling and Optimization of a Subsea Oil-Water Separation System

Master's Thesis

by
Preben FürstTyvold

Co-supervisor: Prof. Sigurd Skogestad

Trondheim, June 11, 2015

Abstract

Compact oil-water separators are essential for treatment of the production streams of oil fields at deep waters. The aim of this work has been to develop a model for a compact oil-water separation system for optimization and control purposes. For these regards, the model is required to be relatively simple in order to achieve low computational costs.

We have studied a system containing a gravity separator for the bulk separation of water and oil, and two inline swirl separators that are connected to it for further purification. One of the swirl separators is used to purify the water-rich product (oil-in-water emulsion) and the other one is used to purify the oil-rich product (water-in-oil emulsion). The separation system has been optimized for different inlet water cuts and flow rates. The optimization variables are the ratio between the product streams of each of the three separators.

The models for the horizontal gravity separator and two co-current, in-line swirl separators have been developed and implemented in MATLAB. The models are based on a characteristic droplet size; the separation rate is given by the average terminal velocity, which is determined by the density difference of the dispersed and the continuous phase and the frictional force given by Stokes' law. The swirl separators use static swirl elements to generate swirling flows that facilitate separation. They are modeled with an inner forced vortex and an outer free vortex, which determine the centrifugal force on the dispersed droplets. The model for the swirl separator with oil-in-water emulsion in the inlet flow is compared to experimental data available in the literature and shows good agreement at different operational conditions.

Sammendrag

Kompakte olje-vann separatorer er viktige for bearbeidingen av produksjonsstrømmer fra oljefelt på dypt vann. Målet for dette arbeidet har vært å utvikle en modell for et kompakt olje-vann separasjonssystem som kan brukes til optimaliserings og regulerings formål. Det er derfor ønskelig med en relativt enkel modell som ikke krever tunge beregninger.

Vi har jobbet med et system som består av en gravitasjonsseparator, som gjøre den grove separasjonen av olje og vann, og to sentrifugal separatorer som er koblet på utløpsstrømmene for videre rensing. Én sentrifugal separator renser det vannrike produktet (olje-i-vann emulsjon) mens den andre renser det oljerike produktet (vann-i-olje emulsjon). Separasjonssystemet har blitt optimalisert for ulike vannfraksjoner og gjennomstrømningsmengder. Optimaliseringsvariablene er forholdet mellom produktstrømmene i hver av de tre separatorene.

Modellene for en gravitasjonsseparator og to medstrøms, sentrifugal separatorer har blitt utviklet og implementert i MATLAB. Modellene er basert på karakteristiske dråpestørrelser; separasjonshastigheten er gitt av den gjennomsnittlige dråpehastigheten, som er beregnet fra oppdriftskraften og friksjonskraften gitt av Stokes' lov. Sentrifugal separatorene bruker statiske *virvelelementer* som generer virvelstrømmer og dermed fremmer separasjonen. Strømningsmønsteret er modellert som en ytre fri virvel og en indre tvungen virvel; dette avgjør sentrifugalkraften som virker på de dispergerte dråpene. Modellen for sentrifugal separatoren for olje-i-vann emulsjoner er sammenlignet med eksperimentelle data og viser god overenstemmelse ved flere ulike driftsbetingelser.

Preface

This master's thesis was written as the final part of the study program of chemical engineering at the Norwegian University of Science and Technology (NTNU). The thesis is written for the Process Systems Engineering group at the Department of Chemical Engineering.

I would like to thank my supervisor, Associate Prof. Johannes Jäschke, for encouragement, advice and productive discussions. I would also like to thank my co-supervisor, Prof. Sigurd Skogestad, for guidance and for letting me be a part of the Process Systems Engineering group, which has been an inspiring experience. I am also grateful to all my friends and fellow students for vital coffee breaks and for contributing to a great student environment, both academically and socially.

Declaration of Compliance

I declare that this is an independent work according to the exam regulations of the Norwegian University of Science and Technology (NTNU).

Trondheim, Norway
June 11, 2015

Preben Fürst Tyvold

Contents

List of Figures

List of Tables

List of Symbols

Latin Letters

Symbol	Description	Unit
A	Cross section area	m^2
A_d	Reference area of droplet	m^2
a	Pylonomial coefficient	–
a_c	Centrifugal acceleration	$\mathrm{m\,s}^{-2}$
b	Pylonomial coefficient	–
C	Concentration	$\mathrm{mol\,m}^{-3}$
C_D	Drag coefficient	–
C_{decay}	Decay factor for lost momentum	–
c	Pylonomial coefficient	–
D	Diffusion coefficient	m
D_d	Diameter of droplet	$\mathrm{m}^2\,\mathrm{s}^{-1}$
F_d	Drag force	N
F_g	Gravitational force	N
FS	Flow split	–
$\vec{FS}$	Vector of flow splits	–
g	Gravitational acceleration (≈ 9.81)	$\mathrm{m\,s}^{-2}$
h	Vertical distance traveled by droplet	m
H_w	Height of weir	m
L	Length of separator	m
p	Pressure	Pa
q	Volumetric flow rate	$\mathrm{m}^3\,\mathrm{s}^{-1}$
R	Radius of separator	m
R_c	Radius of core with solid body rotation	m

Symbol	Description	Unit
R_i	Radius of inner pipe in swirl separator	m
r	Radial coordinate	m
r_{in}	Radial position at inlet	m
r_d	Characteristic droplet radius	–
Re_d	Reynolds number of droplet	–
t	Time	s
V	Volume	m^3
v	Velocity	$m\,s^{-1}$
x	Spatial coordinate	m
z	Spatial coordinate	m

Greek Letters

Symbol	Description	Unit
α	Oil volume fraction / Oil cut	–
β	Smoothing parameter	–
Δ	Difference in the variable that follows	–
η_{dil}	Dilute Efficiency	–
η_{dis}	Dispersed Efficiency	–
θ	Angle of swirl element vanes on z-direction	rad
θ	Angular coordinate	rad
μ	Viscosity	Pa s
π	Ratio of a circles circumference to its diameter	–
ρ	Density	kg/m^3
τ	Residence time	s
φ	Volume fraction of dispersed phase	–
Ω	Swirl number	$rad\,s^{-1}$

List of Subscripts/Superscripts

Acronyms	Description
b	bulk velocity / bottom product of gravity separator
c	Continuous phase
DO	Deoiler
DW	Dewaterer
d	Droplet / Dispersed phase
e	Emulsion
$fixed$	Fixed value
G	Gravity separator
HPO	Heavy phase product
$H, Prod$	Heavy phase product
h	Horizontal direction
in	Inlet stream to separator / separation system
LPO	Light phase product
$L, Prod$	Light phase product
m	Mixture
max	Maximum
o	Oil
opt	Optimal value
$re\text{-}en$	Re-entrainment
t	Top product of gravity separator
v	Vertical direction
v	Vanes of swirl element
w	Water
0	Initial (at $t = 0$ or $z = 0$)
$'$	Prime: Before re-entrainment is considered

List of Acronyms

Acronyms	Description
CFD	Computational fluid dynamics
DO	Deoiler
DW	Dewaterer
HPO	Heavy phase product
LPO	Light phase product
OC	Oil cut / oil volume fraction
RK	Runge-Kutta
WC	Water cut / water volume fraction

1 Introduction

There is an increasing demand for subsea separation in the oil and gas industry [9, 10]. Subsea separation allows fields with lower economic potential (e.g., lower reservoir pressures, deeper waters, etc.) than earlier to be used or considered for oil production [9, 17]. The operating costs are reduced by avoiding the use of energy to pump the produced water to the surface and rather pump it back down into the reservoir or release it into the sea [17]. Reduced operating costs prolong the period of time in which production is economically favorable and thus increase the recovery and economic potential of the field. The need for large platforms is also reduced and the oil from several smaller reservoirs can be separated on the seabed before being pumped up to one common topside facility (e.g., platform, FPSO, etc.).

With the benefits of subsea separation comes several challenges. The reduced accessibility leads to difficulties in maintenance and changing out equipment parts [10, 17]. The subsea separators also have stricter limitations when it comes to size compared to topside separators [9]. The separators have to be lowered down to the seabed by ship cranes in moving, and sometimes deep, waters, which makes large processing units undesirable to use. The small sizes of the separators lead to control challenges due to short residence times and optimization becomes more vital because of the reluctance to oversize the equipment [10]. In addition, changes in the operating conditions during the lifetime of the field need to be dealt with, which makes automation important.

The subsea separators can be optimized by finding the operational conditions that maximize the economic potential of the field and/or minimize the environmental impact. Optimizing the process require accurate, but relatively simple models in order to achieve low computational costs. Models based on first principles have an advantage over purely empirical models in that they can explain why the system behaves as it does. It can therefore predict the response of a disturbance whiteout doing a physical test in advance. This is a valuable quality for a model of a subsea separator as the feed properties (e.g., viscosity, water cut, etc.) usually change over time.

1.1 Objective

The main objective for this thesis has been to develop models for compact oil-water separators. These models are based on first principles and contain only a few empirical parameters and correlations. The modeled separators are co-current swirl separators that use centrifugal forces to facilitate separation. One is developed for oil-rich feed streams (water-in-oil emulsions) and the other for water-rich feed streams (oil-in-water emulsions). The models for the swirl separators are combined with a model for a gravity separator to form a separation system, which is optimized for different inlet water cuts and flow rates.

1.2 Previous Work

This thesis is an extension of a *Specialization Project* carried out in the fall of 2014. The project involved studies of different compact separators and modeling of liquid-liquid separators. The models presented in this

Master's Thesis are based on the models developed in the Specialization Project, but several changes and improvements are implemented succeeding the project. This paper is based on the report written in the context of the Specialization Project and some of the content is reused.

2 Separation Theory

This chapter covers some of the basic concepts in separation theory. This includes sedimentation, diffusion and coalescence (Chapter 2.1-2.3). Though some of the concepts described in this chapter are not explicitly used in the models, the understanding of them is important to assess the impact of neglecting them.

A short description of a swirl element, used in co-current swirl separators, is presented in Chapter 2.4. The used measures of the separation efficiency are defined in Chapter 2.5.

2.1 Sedimentation

When the dispersed liquid in an emulsion has a density that differs from the density of the continuous phase, it will sediment or cream due to gravitational forces. A droplet with density ρ_d and volume V_d in a medium with density ρ will be exposed to the gravitational buoyancy force [11]:

$$F_g = V_d(\rho_d - \rho)g \tag{2.1}$$

Where g is the gravitational acceleration, which can be replaced by an alternative value if the driving force is something else than gravity (e.g., centrifugal force). The frictional force, F_d, on an object moving through a fluid is given by [7]:

$$F_d = -\frac{1}{2}C_D A_d \rho |v| v \tag{2.2}$$

Where C_D is the drag coefficient, A_d is the reference area of the object and v is the relative velocity of the object to the surrounding fluid. The

drag coefficient is dependent on the relative velocity of the object to the surrounding fluid. For laminar flow (i.e., $Re \ll 1$) the drag coefficient is given by Stokes' law [11]:

$$C_D = \frac{24}{Re_d} \tag{2.3}$$

For a spherical droplet, the droplet Reynolds number, Re_d, is defined as;

$$Re_d = \frac{\rho v D_d}{\mu} \tag{2.4}$$

where D_d is the droplet diameter and μ is the viscosity of the fluid. If the droplet velocity increases and the flow regime is in the transition region between laminar and turbulent flow, the drag coefficient deviates from Stokes' law. In this region, a more accurate expression for the drag coefficient is given by equation 2.5 [7]. This means that there is no longer a linear relationship between the drag force and the droplet velocity.

$$C_D = \frac{24}{Re_d}\left[1 + 0.1 Re_d^{0.75}\right] \tag{2.5}$$

However, if Stokes' law is assumed valid (i.e., laminar flow around the particle), equation 2.1, 2.2, 2.3 and 2.4 can be combined to give en explicit expression for the terminal velocity of the droplet:

$$v = \frac{2r_d^2(\rho_d - \rho)g}{9\mu} \tag{2.6}$$

2.1.1 Viscosity of Emulsions

The terminal velocity of a droplet in a gravity driven separator is inversely proportional to the viscosity of the mixture (eq. 2.6). The viscosity of an oil-water emulsion is, among other things, dependent on the droplet size of the dispersed phase and the oil-water ratio [1, 20]. The viscosity typically has a peak at the point of phase inversion as illustrated in Figure 2.1.

Since the goal for an oil-water separator is to move the droplets from one continuous phase to another, they will have to travel through the bulk interface. The composition close to the bulk interphase will typically be close to the phase inversion composition (i.e., the mixture viscosity is high) and this will reduce the separation rate.

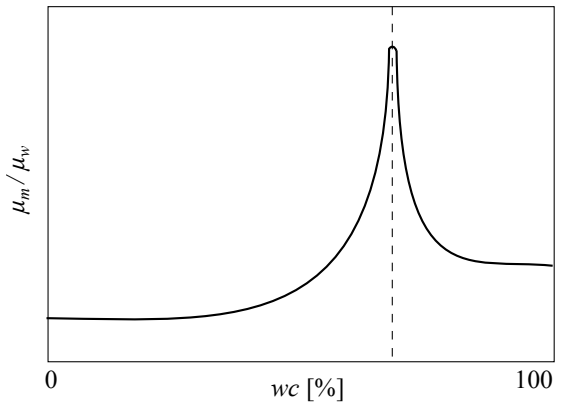

Figure 2.1: Qualitative illustration of the relative viscosity in an oil-water emulsion as a function of the water cut, wc. The relative viscosity is the ratio between the mixture viscosity, μ_m, and the viscosity of pure water, μ_w. The vertical, dashed line represents the phase inversion point. For a more detailed illustration see Arirachakaran et al. [1].

The mixture viscosity is also dependent on the tightness of the emulsion. The tightness of an emulsion is a qualitative term describing the droplet sizes, where a tighter emulsion contains smaller droplets than a loose one. The viscosity increases with the tightness of the emulsion and this effect increases as the oil-water approaches the point of phase inversion [20]. This effect is illustrated qualitatively for a water-in-oil emulsion in Figure 2.2. The droplet sizes (i.e., tightness) of the emulsion entering a separator is typically dependent on the characteristics of the crude oil and the degree

of turbulence it is exposed to upstream of the separator. The effect of turbulence means that the tightness, and thus the viscosity, of the emulsion may change as a function of the process variables (e.g., flow rates) in the separation system leading to difficulties in predicting the separation rate.

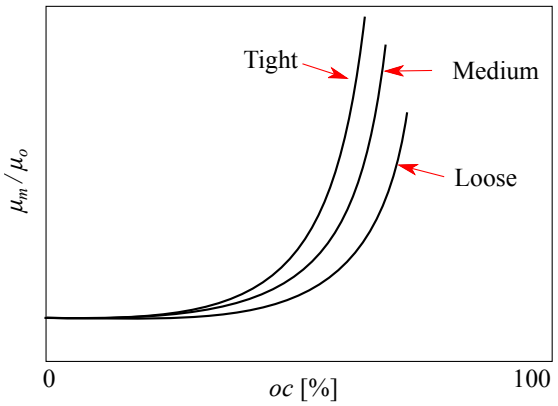

Figure 2.2: Qualitative illustration of the relative viscosity in a water-in-oil emulsion as a function of the oil cut, oc, for three emulsions with different tightness. For a more detailed illustration see Woelflin [20].

Woelflin [20] concluded that the effect of the oil-water ratio on the mixture viscosity is large compered to the effect of the tightness. He also claimed that even though many formulas for predicting the viscosity of emulsions exist, none of them are applicable over the wide range of conditions found in oil fields. By neglecting the effect of the emulsion tightness, equation 2.7 [14] can be used to express the mixture viscosity, μ_m, by fitting the coefficients a, b and c to known data for a particular emulsion.

$$\mu_m = \mu_c \left(1 + a\varphi + b\varphi^2 + c\varphi^3\right) \tag{2.7}$$

Here, μ_c is the viscosity of the continuous phase and φ is the volume fraction of the dispersed phase.

2.2 Diffusion

As soon as the separation process starts due to sedimentation there will arise concentration gradients in the direction of separation. This again will lead to diffusion by Brownian motions, which will have an opposing effect on the separation. The diffusion in an emulsion with a concentration difference in the x-direction can be expressed by Fick's 2. law [11];

$$\frac{dC(t,x)}{dt} = D\frac{\partial^2 C(t,x)}{\partial x^2} \tag{2.8}$$

where D is the diffusion constant for the given system and $C(t,x)$ is the concentration of the dispersed phase.

2.3 Coalescence

Coalescence will occur in a separator as two droplets that melt together, Figure 2.3a, and as droplets melting together with the corresponding continuous phase through the bulk interface, Figure 2.3b. The first is a result of droplets having different velocities caused by, e.g., different sedimentation velocities, diffusion, turbulence, etc. This again leads to collisions, which may cause them to coalesce dependent on the kinetic energy of the droplets and the attractive and repulsive forces between them. Coalescence of droplets increases the sizes of the droplets and thus causes increased separation through sedimentation.

Coalescence of droplets through the bulk interface is necessary in

order to separate out the droplets from the surrounding phase. In cases where the interfacial tension is high, this process can become rate determining for the separation process and droplets will accumulate close to the bulk interface.

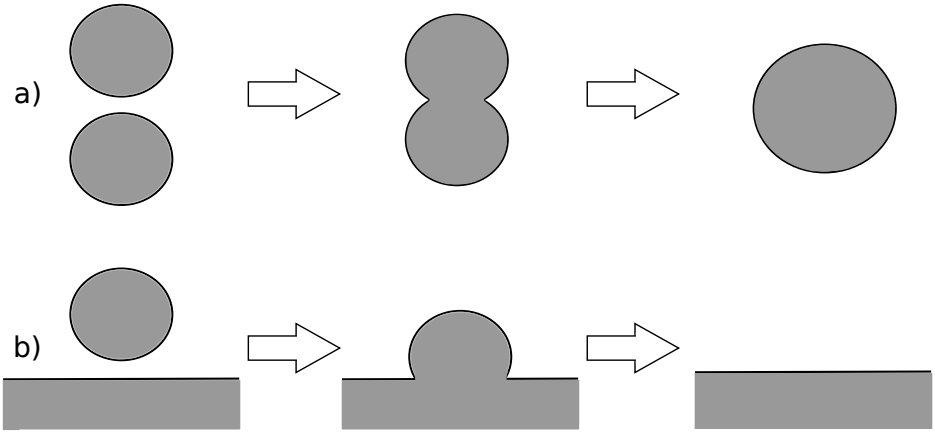

Figure 2.3: **a)** Two droplets coalesce to form one bigger droplet.
b) A droplet coalesce with the bulk phase.

2.4 Swirl Element

This thesis contains models for two swirl separators that use static swirl elements (Figure 2.4) to generate swirling flow (Chapter 3). The swirling flow introduces centrifugal forces acting on the dispersed droplets, which increase the sedimentation velocity [5, 19]. The velocity of the liquid downstream of the swirl element can be decomposed into a tangential and an axial velocity. The relationship is given by [16];

$$\frac{v_{\theta,v}}{v_{z,v}} = \tan(\theta) \tag{2.9}$$

where $v_{\theta,v}$ is the tangential velocity of the liquid at the end of the vanes of the swirl element; $v_{z,v}$ is the axial velocity at the same location and θ is the angle of the vanes to the axial direction.

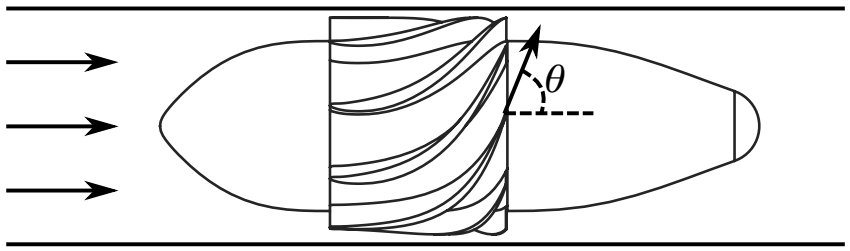

Figure 2.4: Static swirl element. The direction of flow is from left to right. The vanes have an angle (θ) on the axial direction, which introduces the swirling flow. Figure adapted from van Campen [18].

2.5 Separation Efficiency

To evaluate the performance of a separator, it is helpful to define measures of the separation efficiency. In this thesis, the dilute and dispersed efficiencies are used. Considering a separator with an *inlet stream*, a *light phase outlet* (LPO) and a *heavy phase outlet* (HPO). The dilute efficiency, η_{dil}, is defined as the fraction of oil that is kept in the LPO, see eq. 2.10, and can also be referred to as *the recovery of oil*. The dilute efficiency is *one* if there is no oil in the HPO. It is *zero* if there is no oil in the LPO, which in practice means that all the product must be taken out in the HPO. It is important to consider the dilute efficiency if the aim is to minimize the loss of oil.

$$\eta_{dil} = \frac{\alpha_{LPO}\ q_{LPO}}{\alpha_{in}\ q_{in}} \tag{2.10}$$

Where α_i and q_i are the oil volume fraction and volumetric flow rate in stream i, respectively.

The dispersed efficiency, η_{dis}, is a measure of how much of the liquid that exits through the desired outlet, eq. 2.11. The dispersed efficiency is *one* if the HPO stream is pure water and the LPO stream is pure oil, which is the desired performance of any separator.

$$\eta_{dis} = 1 - \frac{(1 - \alpha_{LPO})\ q_{LPO} + \alpha_{HPO}\ q_{HPO}}{q_{in}} \tag{2.11}$$

3 Model Description

This chapter addresses the principles and assumptions made around the models for three different separators. The models for;

1. a swirl separator for oil-in-water emulsions
2. a swirl separator for water-in-oil emulsions
3. a gravity separator

are covered in Chapter 3.1, 3.2 and 3.3, respectively. These steady-state models are quite simplistic and are meant to give relatively rough estimates of the composition in the outlet streams given a set of inlet conditions. They are, in essence, based on how the buoyancy forces affect the path of an averaged sized droplet through the separators.

The separator models require certain sets of input variables and correlations to produce outputs. These inputs include the separator dimensions and the properties of the emulsion. The inputs used to analyze the behavior of the models are presented and discussed in Chapter 3.4.

A hypothetical separation system consisting of three modeled separators are described in Chapter 3.5. This separation system is studied to see how the modeled separators interact, and is optimized for the quality of the oil-rich product (for optimization procedure, see Chapter 4).

3.1 Swirl Separator for Continuous Water Phase

The model for the co-current swirl separator is based on centrifugal buoyancy forces acting on the oil droplets, which are represented by the average droplet size.

The inlet stream passes the swirl element (described in Chapter 2.4) and flows through the separator with a swirling flow pattern. The density difference between the oil droplets and the continuous water phase causes the droplets to be pushed towards the center of the separator (see Figure 3.1). At the end of the separator there is a light phase outlet (LPO) with radius $R_i < R$ where the inner fraction of the flow is extracted while the liquid outside of this radius passes the pick-up tube and exits through the heavy phase outlet (HPO).

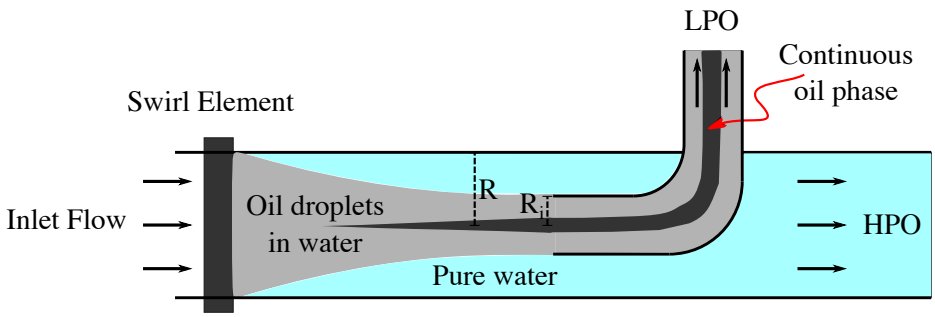

Figure 3.1: The swirl element introduces a rotation in the liquid, which facilitates a swirling flow through the separator. The inlet flow is separated by centrifugal buoyancy forces to the light phase outlet (LPO) and the heavy phase outlet (HPO).

The following sections describe the major assumptions made for the model of the swirl separator for oil-in-water emulsions. These include the axial, tangential and radial velocities, the viscosity, the re-entrainment and the numerical estimation of the outlet compositions. Section 3.1.8 provides a short summary of this general model.

3.1.1 Axial Velocity

The flow rates through the two outlets can be manipulated by adjusting valves on either of the streams. The flow split, FS, is defined in equation 3.1.

$$FS = \frac{q_{LPO}}{q_{in}} \tag{3.1}$$

Where q_{in} and q_{LPO} are the volumetric flow rates at the inlet and at the light phase outlet, respectively.

Depending on the flow split, the axial velocity in the center of the pipe might be greater or smaller than in the outer part of the pipe. It is assumed that the axial velocity profile can be divided into two regions with constant velocity, one for $r \leq R_i$ and one for $r > R_i$. The axial velocity is then given by equation 3.2 and is illustrated in Figure 3.2. This assumption implies that there is neither friction between the cylindrical and the annular plug flow, nor between the fluid and the pipe wall. It also means that the axial velocity is unaffected by the swirling character of the flow. In addition, turbulence is neglected by using time-averaged velocities.

$$v_z(r) = \begin{cases} \frac{q_{LPO}}{\pi R_i^2}, & 0 \leq r \leq R_i \\ \frac{q_{HPO}}{\pi(R^2 - R_i^2)}, & R_i < r \leq R \end{cases} \tag{3.2}$$

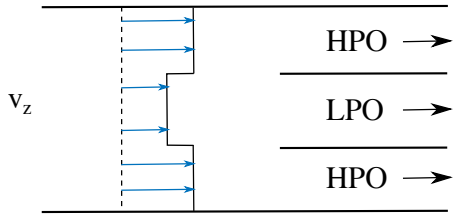

Figure 3.2: Axial velocity profile in the swirl separator. In this example the pressure is greater at the LPO than at the HPO. This means that $FS < (R_i/R)^2$ so the axial velocity is greater on the outside of the inner pipe than on the inside.

Note that the axial velocity profile is significantly simplified compared to how it is expected to be in reality. However, the approximation of axial velocity of the droplets is expected to be good since the aim is to estimate the separation performance. The axial velocity mainly affects the separation performance by determining the residence time of the droplets, in which case the average velocity is assumed to be sufficient. This is a simplification as the radial velocity of a droplet is a function of its radial position, but the approximation is expected to give a relatively good estimate.

3.1.2 Tangential Velocity

The centrifugal acceleration is the driving force of the separation and is given by;

$$a_c(r) = \frac{v_\theta(r)^2}{r} \tag{3.3}$$

where v_θ is the tangential velocity of the fluid. Experimental data show that the tangential velocity in a swirl separator can be well described

as a Rankine vortex [5, 12, 19]. This means that the velocity profile can by divided it into an inner region with a solid body rotation and an outer region that moves like a free vortex. The velocity profile is simplified by assuming constant velocity in the outer region, which shows good agreement with experimental data [18]. The distinction between the inner and the outer region is at some radius R_c as illustrated in Figure 3.3.

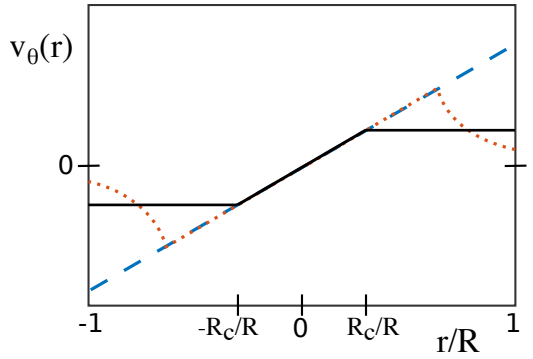

Figure 3.3: Tangential velocity , v_θ, as a function of radial position r in a swirl separator with radius R. Solid line: Used approximation, Dashed line: No drag from wall, Dotted line: Rankine vortex.

The tangential velocity right downstream of the swirl element, v_θ^0, is thus given by equation 3.4. Note that for the oil-in-water separator considered in this work, the radius of the inner pipe is greater than R_c (i.e., $R_i > R_c$, see Chapter 3.4.2). This means that only the constant tangential velocity is used in the model as the droplet is simulated from the inlet radial position ($r_{in} > R_i$) to R_i.

$$v_\theta^0(r) = \begin{cases} v_\theta^{max} \frac{r}{R_c} & , 0 \leq r \leq R_c \\ v_\theta^{max} & , R_c < r \leq R \end{cases} \tag{3.4}$$

Where v_θ^{max} is the maximum tangential velocity that is assumed to be proportional to the bulk velocity in the axial direction, $v_{z,b}$:

$$v_\theta^{max} = \Omega v_{z,b} \tag{3.5}$$

The proportionality constant Ω can be calculated from the geometry of the swirl element or measured experimentally. In this work, Ω is referred to as the *swirl number* even though that term is used with a slightly different meaning in other papers found in the literature [5, 18]. The swirling flow is expected to lose momentum due to stress from the pipe wall. This is accounted for by introducing a decaying factor such that the tangential velocity, $v_\theta(r, z)$, is given by [5, 12, 16];

$$v_\theta(r, z) = v_\theta^0(r) e^{\frac{-C_{decay} z}{2R}} \tag{3.6}$$

where C_{decay} is a parameter that can be determined experimentally.

3.1.3 Radial Velocity

By assuming that the fluid is in the Stokes' regime (equation 2.6), the radial velocity of a droplet, v_r, can be expressed as in equation 3.7. This is the relative velocity of the droplet to the continuous phase, but is used as the approximated absolute velocity by neglecting the radial movement of the continuous phase. This involves neglecting all turbulence in the radial direction. Note that the terminal velocity is used (i.e., the acceleration time is neglected).

$$v_r(r, z) = \frac{2r_d^2(\rho_d - \rho)}{9\mu(r, z)} \frac{v_\theta^2(r, z)}{r} \tag{3.7}$$

Where r_d is the radius of the droplet, μ is the viscosity of the emulsion and ρ_d and ρ are the densities of the dispersed and continuous phases,

respectively. Equation 3.7 takes only the centrifugal buoyancy force into account; other mass transport phenomena (e.g., diffusion) will affect the radial movement of the droplets, but the centrifugal acceleration in a swirl separator is generally large ($> 100g$ [16]) and is assumed to be the dominating effect.

3.1.4 Viscosity and Concentration

As the droplet moves downstream in the separator, it is pushed towards the center of the cylinder. Since the viscosity of an oil-water emulsion is a function of the oil volume fraction (see section 2.1.1) and the oil volume fraction is a function of the axial and radial coordinates, the viscosity is dependent on the position of the droplet.

It is assumed that the viscosity can be estimated at any point along the droplet path using the average oil volume fraction between the droplet and the center of the separator, $\alpha_c(r, z)$. Considering a droplet entering the separator at $r = r_{in}$ and exiting at $r = R_i$, at any position r on the droplet path, α_c is given by equation 3.8. This expression is derived in Appendix A.

$$\alpha_c(r, z) = \alpha_{in} \frac{FS(R^2 - R_i^2) + (1 - FS)(r_{in}^2 - R_i^2)}{(1 - FS)(r^2 - R_i^2) + FS(R^2 - R_i^2)} \tag{3.8}$$

Where α_{in} is the oil volume fraction at the inlet of the separator. The assumptions made are that the distribution of oil is uniform at the inlet and that no droplet paths cross each other in the separator. That is, all droplets entering at $r < r_{in}$ stay on the inside of the droplet path and all droplets entering at $r > r_{in}$ stay on the outside. The resulting concentration profile through the separator is illustrated in Figure 3.4. In reality,

the oil volume fraction is expected to increase gradually from the pipe wall to the center of the separator [16]. Since the model uses the average concentration between the droplet and the center of the separator, the oil volume fraction, and thus the viscosity, is expected to be overestimated.

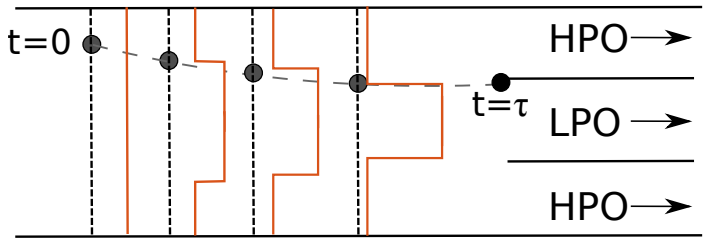

Figure 3.4: Approximation of the oil volume fraction (red lines) as a function of r for four different values of z. A droplet enters the separator at $t = 0$ and $r = r_{in}$ and exits at $t = \tau$ and $r = R_i$. At any position on the droplets path, the oil volume fraction on the inside and outside of the droplet is assumed constant in r.

By neglecting the dependency of the viscosity to the emulsion tightness (see section 2.1.1) and assuming constant temperature, the viscosity of an emulsion of a given oil and brine can be formulated as a function of the oil volume fraction. The emulsion will at some point in the separator submit to a phase inversion, where the oil phase becomes continuous. This transformation is not estimated in the model; it is assumed that the viscosity function for continuous water phase is sufficient even if the phases, in reality, are inverted. In this work the viscosity has been estimated by fitting equation 2.7 to experimental data, but other methods can be used depending on what data that are available.

3.1.5 Average Droplet Size

The average droplet size is assumed to be a function of the maximum tangential velocity present in the separator. Droplet break-up is expected to happen predominately by the acceleration of the fluid at the swirl element and the acceleration of the droplets in the radial direction due to the centrifugal buoyancy forces [16, 18]. Both effects are related to the tangential velocity. There exist theoretical expressions for the maximum droplet size that can withstand a given flow [4, 6], but as knowing the average droplet size is necessary for the model, experimental correlations are used. Since the droplet stability is, to a great extent, affected by the interfacial tension of the droplet [6], this correlation is dependent on the type of oil and brine present in the system.

Note that the word *average* in the context of droplet sizes, in this thesis means the *volume average*.

3.1.6 Solving the Equation of Motion

The goal for the model is to find the radial inlet position (r) of the droplet that exits the separator at $r = R_i$. The droplet will travel with an axial velocity given by equation 3.2 and a radial velocity given by equation 3.7. The residence time of the droplet, τ, is given by the axial velocity and can by written as;

$$\tau = \frac{\pi \left(R^2 - R_i^2\right) L}{(1 - FS)\, q_{in}} \tag{3.9}$$

where L is the distance between the swirl element and the inner pipe.

The outlet position of a droplet entering the separator at any ra-

dial position is found by integrating the radial velocity (equation 3.7) from $t = 0$ to $t = \tau$ in MATLAB. To save computational costs, this is done by a constant time step, second order, explicit Runge-Kutta integrator [3]. The integral time is divided into 10 equal time steps $\Delta t = \tau/10$. The radial position of the droplet (r_{n+1}) is calculated from the previous position (r_n):

$$k_1 = v_r(t_n, r_n)\Delta t \tag{3.10}$$

$$k_2 = v_r(t_n + \Delta t, r_n + k_1)\Delta t \tag{3.11}$$

$$r_{n+1} = r_n + \frac{k_1 + k_2}{2} \tag{3.12}$$

Where $v_r(t, r)$ is the radial velocity of the droplet. The constant time step Runge-Kutta integrator shows good agreement with other integrators in MATLAB, and a significant reduction in computational costs (see Appendix B). Full details of the used MATLAB function can be found in Appendix C.5.1.

Since the expression for the viscosity (eq. 3.8), and thus the radial velocity, is a function of the radial inlet position of the droplet and the radial outlet position is fixed, the governing differential equation is a boundary value problem. The particular inlet position that leads to the droplet exiting at $r = R_i$ can be found by use of the *shooting method*, which uses the Newton-Raphson method to solve the boundary value problem [3]. The MATLAB function used for the *shooting method* is available in Appendix C.5.2. When using the *fmincon* function in MATLAB, the boundary value problem can be solved by setting the inlet position as a state and the outlet position as an additional equality constraint.

When the inlet position (r_{in}) of the droplet that exit at $r = R_i$ is found, the LPO oil volume fraction can be calculated by assuming that all droplets entering on the inside of this droplet (i.e., at $r < r_{in}$) will go to the LPO. Correspondingly, all droplets entering on the outside of this particular droplet (i.e., at $r > r_{in}$) will exit through the HPO. Assuming that the distribution of oil droplets in the radial and tangential direction is uniform at the inlet, the oil volume fraction in the LPO, α'_{LPO}, is given by equation 3.13. The expression is found by replacing r in equation 3.8 with R_i.

The *min* function simply states that the oil volume fraction cannot be greater than one (i.e., $\alpha \leq 1$). If the amount of oil that has travelled the necessary distance is greater than the flow rate through the LPO, the oil core will simply grow wider than the radius of the inner pipe (R_i) and the residual oil will exit through the HPO. The oil volume fraction in the HPO, α'_{HPO}, is then given by the mass balance of oil as in equation 3.14. Note that these oil volume fractions are later adjusted when taking re-entrainment into account and are therefore marked with primes.

$$\alpha'_{LPO} = min\left[1, \alpha_{in}\frac{FS\left(R^2 - R_i^2\right) + (1 - FS)\left(r_{in}^2 - R_i^2\right)}{FS\left(R^2 - R_i^2\right)}\right] \tag{3.13}$$

$$\alpha'_{HPO} = \frac{\alpha_{in} - \alpha'_{LPO}FS}{1 - FS} \tag{3.14}$$

3.1.7 Re-Entrainment

Re-entrainment is included in the model to compensate for the oversimplification of the velocity profiles. The assumption made in section 3.1.1 is that the axial flow can be divided into two regions that move with two different constant velocities. This means that there is no net flux across

the boundary between the regions (located at $r = R_i$). In reality this assumption is not completely accurate and if the pressure is lower at the LPO than at the HPO, some liquid will be pulled across the boundary from $r > R_i$ to $r < R_i$ and exit through the LPO (and vice versa if $p_{HPO} < p_{LPO}$). This is illustrated in Figure 3.5. Simulations done with CFD (Computational Fluid Dynamics) by Slot [16] confirms this type of flow pattern and even show regions in which the liquid flows upstream. This is also measured experimentally by van Campen [18].

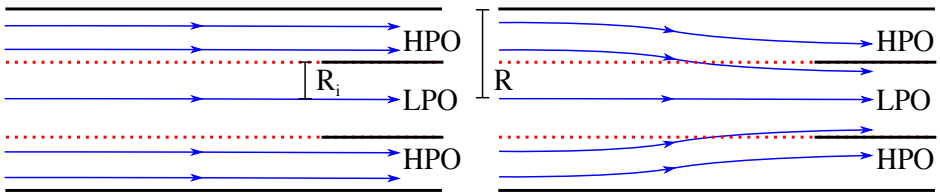

Figure 3.5: Streamlines (blue) at the end of the separator for a case where the pressure at the LPO is lower than at the HPO ($FS > (R_i/R)^2$).
Left: How the streamlines look according to the model. There is no net flow in the radial direction.
Right: A more realistic case where there is net flow going towards the center of the separator. Note that this is still a simplification and that the actual flow pattern can be significantly more complex.

The concept described above means that some of the water thought to be separated from the oil will be re-entrained with the light phase product (and vice versa for low flow splits). It is reasonable to assume that the amount of re-entrained liquid will increase when the difference in the axial velocities in the LPO and the HPO increases. The re-entrainment rate, $q_{re\text{-}en}$, has been investigated with different relationships to the velocity difference (see Appendix D). The linear relationship stated in equation 3.15

showed the best agreement with experimental data.

$$q_{re\text{-}en} = k_{re\text{-}en}\Delta v \tag{3.15}$$

Where $\Delta v = v_{LPO} - v_{HPO}$ is the velocity difference between the inner and the outer region and $k_{re\text{-}en}$ is a proportionality constant, which is used as a fitting parameter in the model.

The final oil volume fraction in the light phase outlet, α_{LPO}, is found by adding the re-entrained liquid to the LPO:

$$\alpha_{LPO} = \frac{1}{q_{LPO}}\left[\alpha'_{LPO}\left(q_{LPO} - q_{re\text{-}en}\right) + \alpha'_{HPO}q_{re\text{-}en}\right] \tag{3.16}$$

Note that the flow rate $q_{HPO} = (1 - FS)q_{in}$ is used to represent the outer cylindrical plug flow in the equations previous to this section. If the re-entrainment happens close to the outlet of the separator, a more appropriate flow rate to use is $q'_{HPO} = q_{HPO} - q_{re\text{-}en}$. However, it is desirable to keep the flow split as an input to the model and not a function of the re-entrainment rate. An important assumption is therefore that the rate of re-entrainment is low compared to the HPO flow rate (i.e., $q_{re\text{-}en}/q_{HPO} \ll 1$).

Again, the oil volume fraction of the HPO can be calculated from the mass balance of oil:

$$\alpha_{HPO} = \frac{\alpha_{in} - \alpha_{LPO}FS}{1 - FS} \tag{3.17}$$

3.1.8 Summary of Oil-in-Water Swirl Separator Model

The model described above provides the necessary equations to estimate the oil volume fraction in the outlets (eq. 3.16 & 3.17) given the inlet

composition, flow rate and the flow split of the separator. A prerequisite is that the physical dimensions of the separator are known, including the swirl number. In addition, the model contains three parameters that must be determined (i.e., R_c, C_{decay} & $k_{re\text{-}en}$).

Other inputs to the model are the physical properties of the emulsion. These are the densities of both pure phases, and the viscosity of the mixture as a function of the oil volume fraction. It is assumed that the viscosity is dependent only on the oil volume fraction and all other effects are neglected.

The model is based on the average droplet size and it is assumed that this is sufficient to give a crude estimation of separation performance. Droplet break-up is expected to increase with the swirl intensity and a correlation between the average droplet size and the maximum tangential velocity is required as an input.

3.2 Swirl Separator for Continuous Oil Phase

A model for a swirl separator for water-in-oil emulsions is also developed for this thesis. This type of separator is very similar to the separator for oil-in-water emulsions described in Chapter 3.1. The main difference is that the density of the droplets is greater than the density of the continuous phase so the centrifugal buoyancy forces push the droplets outwards (see Figure 3.6).

In general, this type of separator handles mixtures with higher oil contents so the relative size of the inner pipe to the outer pipe will

typically be larger. This allows for more product to be taken out from the LPO relative to the HPO. Water-in-oil emulsions will normally also have higher viscosities, which may lead to reduced separation performance.

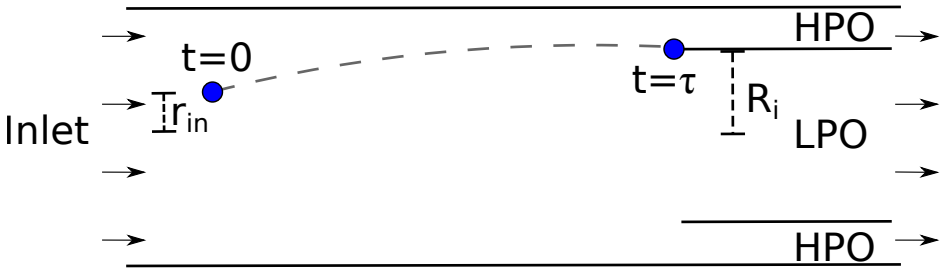

Figure 3.6: Water droplet in a swirl separator with a continuous oil phase. The droplet enters the separator at $t = 0$ and $r = r_{in}$ before it is pushed outwards by the centrifugal buoyancy forces and exits the separator at $t = \tau$ and $r = R_i$.

The velocity profiles in the water-in-oil separator are modeled in the same manner as for the oil-in-water separator. These velocity profiles, and the assumptions made around them, are described in Chapter 3.1.1-3.1.3. A small adjustment in the tangential velocity profile is done for numerical reasons and this is described in Chapter 3.2.1. The only other difference from the oil-in-water separator is that the radial velocity will have the opposite sign due to the inverted phases.

The average droplet size is still assumed to be a function of the maximum tangential velocity present in the separator (see Chapter 3.1.5). An empirical relationship between these two variables is required as an input to the model.

The model also needs an empirical relationship between the viscosity of the mixture and the oil volume fraction. The oil volume fraction is approximated by the average value between the droplet and the pipe wall. This is discussed is Chapter 3.1.4.

Chapter 3.2.1 covers a smoothing approximation applied to the tangential velocity in order to make the model more friendly to numerical solvers. The estimation of the oil volume fractions of the product streams is described in Chapter 3.2.2 before a short summary of the model is presented in Chapter 3.2.3.

3.2.1 Smoothing of the Tangential Velocity Function

It is desirable to have smooth functions with continuous derivatives when performing numerical calculations. The tangential velocity described by equation 3.4 is a non-smooth function with a discontinuous derivative with respect to the radial coordinate. For the oil-in-water swirl separator, this is irrelevant as the region of interest is the outer part, where the function is constant. For the water-in-oil separator, however, droplets are expected to travel from the inner region with a solid body rotation, to the outer region of constant tangential velocity. This can cause problems for the integrator function (see Chapter 3.1.6) and the optimization function (*fmincon*) as they both consider the derivatives. To avoid problems with the solver, the smoothing approximation of Balakrishna and Biegler [2] is used:

$$max\left(f(x),0\right)=\frac{1}{2}\left[\left(f^2(x)+\beta^2\right)^{1/2}+f(x)\right] \tag{3.18}$$

Where β is the smoothing parameter. The tangential velocity, v_θ^0, can be smoothened by rewriting equation 3.4 to equation 3.19 and apply the smoothing approximation.

$$v_\theta^0 = v_\theta^{max} - max\left(v_\theta^{max}\left[1 - \frac{r}{R_c}\right], 0\right) \tag{3.19}$$

A smoothened approximation of the tangential velocity is illustrated in Figure 3.7. In this particular example, the transition from the inner to the outer region is located at $R_c = 0.25R$ and the size of the smoothing parameter is set to 5% of v_θ^{max}. The smoothened approximation follows the original function tightly, except in the region where the original function has a kink. Here, the approximation is smooth, which means that we avoid potential problems with the MATLAB solvers. The deviation of the smoothened function to the original function is negligible and not expected to affect the estimated separation performance considerably.

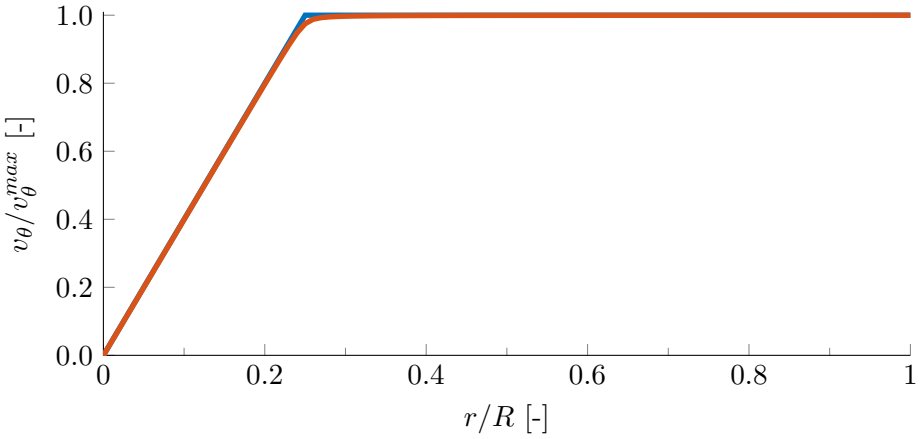

Figure 3.7: Relative tangential velocity as a function of the relative radial coordinate. The blue curve is non-smooth at $r = R_c = 0.25R$. The red curve represents the smooth approximation with $\beta = 0.05 \cdot v_\theta^{max}$.

3.2.2 Oil Cut in the Product Streams

The oil volume fractions in the LPO and HPO are found with the same approach as for the oil-in-water separator. First the radial inlet position of the droplet exiting at $r = R_i$ is found. This is done by integrating the radial velocity (equation 3.7) from $t = 0$ to $t = \tau$. The residence time, τ, is now given by:

$$\tau = \frac{\pi R_i^2 L}{FS \cdot q_{in}} \tag{3.20}$$

The radial velocity is integrated with the second order Runge-Kutta integrator and the boundary value problem is solved with the shooting method (see Chapter 3.1.6 for description of this procedure). It is assumed that the emulsion enters the separator with a uniform distribution of the dispersed phase in the r,θ-plane and that no droplet paths cross each other during the separation process. The water volume fraction of the HPO, $\alpha'_{w,HPO}$, before re-entrainment is then given by:

$$\alpha'_{w,HPO} = (1 - \alpha_{in}) \frac{(1 - FS)R_i^2 + FS\left(R_i^2 - r_{in}^2\right)}{(1 - FS)R_i^2} \tag{3.21}$$

The volume fraction of water in the LPO, $\alpha'_{w,LPO}$, is derived from the component mass balance:

$$\alpha'_{w,LPO} = \frac{1}{q_{LPO}} \left[(1 - \alpha_{in})\ q_{in} - \alpha'_{w,HPO}\ q_{HPO}\right] \tag{3.22}$$

The re-entrainment rate, $q_{re\text{-}en}$, is still assumed to be given by equation 3.15. The water cut in the LPO after re-entrainment, $\alpha_{w,LPO}$, is then given by equation 3.23. This is still under the assumptions discussed in Chapter 3.1.7.

$$\alpha_{w,LPO} = \frac{1}{q_{LPO}} \left[\alpha'_{w,LPO}\left(q_{LPO} - q_{re\text{-}en}\right) + \alpha'_{w,HPO} q_{re\text{-}en}\right] \tag{3.23}$$

Finally, the oil volume fractions of the LPO and the HPO are given by equation 3.24 & 3.25, respectively.

$$\alpha_{LPO} = 1 - \alpha_{w,LPO} \tag{3.24}$$

$$\alpha_{HPO} = \frac{1}{q_{HPO}} \left[\alpha_{in}\ q_{in} - \alpha_{LPO}\ q_{LPO}\right] \tag{3.25}$$

3.2.3 Summary of Water-in-Oil Swirl Separator Model

The model described above predicts the oil volume fraction in the product streams (eq. 3.24 & 3.25) given the inlet composition, flow rate and the flow split of the separator. The model is based on the same principles and assumptions as the model for the oil-in-water swirl separator.

Required inputs to the model are the physical dimensions and swirl number of the separator, the densities of the two phases and a correlation between the viscosity and the oil volume fraction of the emulsion. The model also contains three parameters that must be tuned (i.e., R_c, C_{decay} & $k_{re\text{-}en}$). Additionally, the average drop size as a function of the maximum tangential velocity present in the separator is required.

3.3 Horizontal Gravity Separator

A steady-state model for a horizontal, gravity driven tank separator has been developed for this work. The main focus has been on the swirl separators, but a model for gravity separator has been included in order to do the initial bulk separation in the separation system described in Chapter 3.5.

The gravity separator is a horizontal, cylindrical tank with two outlets, see Figure 3.8. The liquid enters the separator as an oil-in-water emulsion and the gravitational buoyancy forces push the dispersed oil droplets up and the continuous water phase down. This causes a continuous oil phase to be formed at the top of the separator and a pure water phase at the bottom. At the end of a separator there is a vertical weir that separates the flow into two product streams, q_t and q_b. The location of the "top" outlet at the bottom of the separator, behind the weir, allows for an additional gas outlet at the top of the tank. A gas phase has not been included in this particular work as the focus has been on oil-water separation, but it can easily be included in future work.

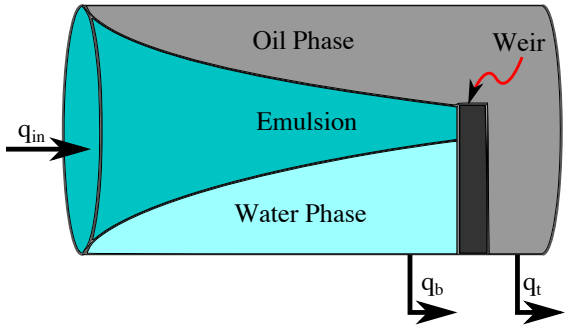

Figure 3.8: Horizontal gravity separator. The liquid enters the separator as an oil-in-water emulsion. As the gravitational buoyancy forces push the oil droplets up, a continuous oil phase is formed in the top of the separator and a pure water phase in the bottom.

The following sections describe the model for the horizontal gravity separator and the main assumptions made in this context. This includes the horizontal and vertical velocities, the droplet sizes and the viscosity in the separator. A summary of the model is presented in Chapter 3.3.6.

3.3.1 Horizontal Velocity

The flow through the separator is modeled as two separate plug flows separated by the height of the weir (H_w), see Figure 3.9. There is assumed to be no net mass transfer between the plug flows, but oil droplets will rise from the lower part to the upper part with equal amounts of water moving in the opposite direction. The liquid that hits the weir at the end of the separator is assumed to exit through the bottom outlet, while the liquid above H_w is assumed to flow over the weir and exit through the top outlet.

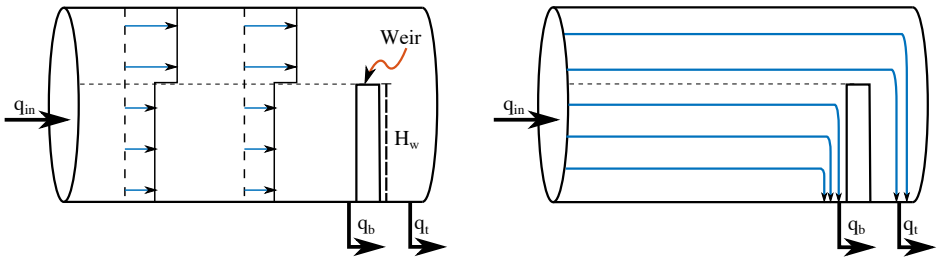

(a) Horizontal velocity profile. **(b)** Stream lines.

Figure 3.9: The modeled horizontal flow in the gravity separator is divided into two regions. The liquid under the weir has a constant horizontal velocity until it hits the weir and exits through the bottom outlet (q_b). The liquid over the weir has another constant velocity and flows over the weir and exits through the top outlet (q_t).

The flow rates of the two plug flows can be manipulated by adjusting valves on either of the outlet streams. The horizontal velocity, v_h, of a droplet moving through the separator under H_w is assumed to be equal to that of the continuous phase and is given by;

$$v_h = \frac{q_b}{A_b} \tag{3.26}$$

where q_b is the volumetric flow rate of the bottom outlet stream and A_b is the cross section area of the lower part of the separator (i.e. the circular segment limited by H_w). This cross section area can be derived from simple trigonometry to be;

$$A_b = \frac{R^2}{2}\left[2\cos^{-1}\left(\frac{R-H_w}{R}\right) - \sin\left(2\cos^{-1}\left(\frac{R-H_w}{R}\right)\right)\right] \tag{3.27}$$

where R is the radius of the separator.

3.3.2 Vertical Velocity

The vertical velocities of the droplets are caused by the gravitational buoyancy forces and are given by equation 2.6 under the assumptions discussed in Chapter 2.1. Equation 2.6 is repeated below.

$$v_v = \frac{2r_d^2(\rho_d - \rho)g}{9\mu(\alpha)} \tag{3.28}$$

Where r_d is the radius of the droplet; ρ_d and ρ are the densities of the droplet and continuous phase, respectively; and g is the gravitational acceleration. The viscosity of the emulsion, $\mu(\alpha)$, is a function of the oil cut, α.

As discussed in Chapter 2.1, v_v is the velocity of the droplet relative to the continuous phase. However, by neglecting the vertical movement of the continuous phase it can be used as an approximation to the absolute velocity. This assumption involves neglecting all turbulence in the vertical direction.

3.3.3 Droplet Size

It is assumed that knowing the average droplet size is sufficient to estimate the separation performance of the gravity separator. The average droplet size is an input to the model and is assumed to be independent of the flow rate. This assumption is in contrast to the models for the swirl separators and is a forced simplification due to a lack of experimental data on the matter. It can be argued that the effect of droplet break-up will be less present in the gravity separator due to the lower velocities. On this basis, the assumption of using a constant droplet size might be reasonable. On the other hand, the droplets will be exposed to more stress in pipes and valves upstream of the separator, which might facilitate droplet break-up. Experimental research on the matter is necessary to validate or improve the model.

3.3.4 Concentration and Viscosity

The separator is divided into three different phases with uniform concentration profiles. The emulsion phase is assumed to have an oil volume fraction equal to that of the incoming fluid, $\alpha = \alpha_{in}$. As the separation process progresses, a pure oil phase is formed in the top and a pure water phases is formed in the bottom of the tank. As the liquid flows downstream in the separator, the emulsion phase shrinks and the two pure phases grow. This assumption is illustrated in Figure 3.10.

The modeled concentration profile is based on the assumption that all the droplets move with the same vertical velocity. As the buoyancy force is proportional to the volume of the droplet, the accuracy of

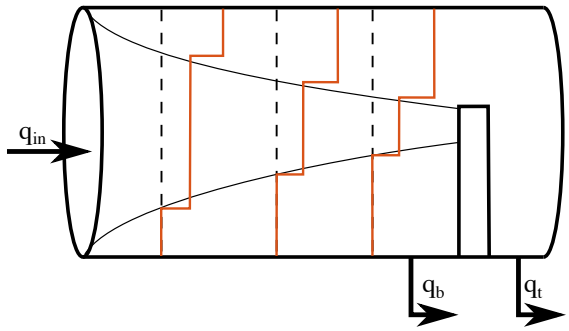

Figure 3.10: Modeled concentration profile in the gravity separator. The red line represents the oil volume fraction, α. The liquid can be divided into three phases:

1. The water phase on the bottom with $\alpha = 0$.
2. The emulsion phase in the middle with $\alpha = \alpha_{in}$.
3. The oil phase at the top with $\alpha = 1$.

this assumption will decrease with increasing standard deviation in the droplet size distribution. It also means that there is no accumulation of oil droplets underneath the oil-emulsion bulk interface. In other words, the coalescence process between the oil droplets and the continuous oil phase (see Chapter 2.3) is fast compared to the sedimentation process. This assumption is based on the sedimentation rate being relatively low ($g \approx 9.8\,\mathrm{m\,s^{-2}} \ll a_c$) and the bulk interface the droplets have to penetrate being relatively large. Note that the subdivision into three phases is *not* done for the swirl separators where the bulk interface is smaller and the time the droplets have to coalesce through this interface is significantly shorter.

The viscosity of the emulsion is assumed to be dependent on the oil volume fraction and the properties of the two liquids. The dependency is expected to be the same as for the oil-in-water swirl separator discussed

in Chapter 3.1.4. The main difference is that the oil concentration in the emulsion for the gravity separator is assumed to be constant. This means that the viscosity in the emulsion phase is dependent only on the oil volume fraction in the inlet stream, i.e. $\mu(\alpha_{in})$.

3.3.5 Oil Cut in the Product Streams

The oil volume fractions of the product streams are estimated by finding the vertical distance, Δh, a droplet entering the separator at the bottom of the tank, travels during its residence time in the separator. A droplet located in the lower part of the separator (bellow H_w) will travel the vertical distance;

$$\Delta h = \frac{v_v}{v_h} L \tag{3.29}$$

where L is the horizontal distance from the inlet to the weir and v_v (eq. 3.28) and v_h (eq. 3.26) are the vertical and horizontal velocities of the droplet, respectively.

If all the droplets move with the same vertical velocity, the situation illustrated in Figure 3.11 arises. Figure 3.11a shows the cross section of the separator at the inlet, where all the liquid is oil-in-water emulsion. Figure 3.11b shows the end of the separator if all the droplets move the same vertical distance, Δh. In reality, the droplets that hit the ceiling will accumulate and form a continuous oil phase in the top as illustrated in Figure 3.11c. Considering that the liquid located above H_w might have a different horizontal velocity than the liquid below H_w, the illustration is not an accurate depiction. The droplets that cross the horizontal plane at the height H_w will have different residence times and thus travel different vertical distances. However, the only information that is necessary to

estimate the outlet composition is the amount of oil droplets that cross this horizontal plane.

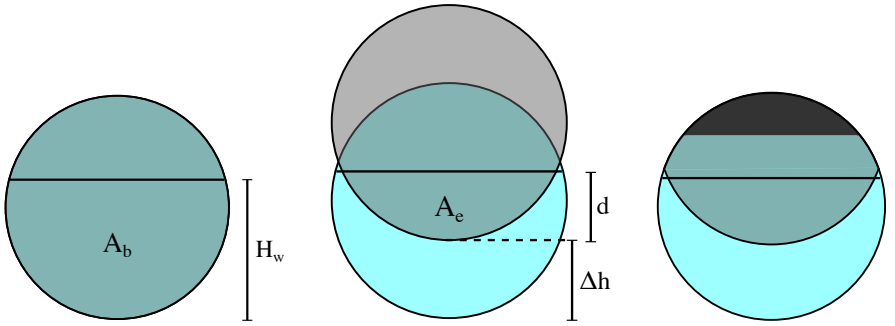

(a) At beginning of separator.

(b) At end of separator. Hypothetical case.

(c) At end of separator. "Actual case".

Figure 3.11: Cross section of gravity separator at the beginning and end of the gravity separator. The emulsion (grey) moves a distance Δh in the vertical direction during the residence time in the separator. A pure oil phase (black) is formed in the top and a pure water phase (light blue) is formed in the bottom of the separator.

The amount of oil left in the bottom part of the tank at the end of the separator is given by the circular segment limited by $d = H_w - \Delta h$, see Figure 3.11b. The area of this circular segment is given by:

$$A_e = \frac{R^2}{2}\left[2\cos^{-1}\left(\frac{R-d}{R}\right) - \sin\left(2\cos^{-1}\left(\frac{R-d}{R}\right)\right)\right] \tag{3.30}$$

The oil volume fraction of the bottom outlet, α_b, is then given by;

$$\alpha_b = \alpha_{in}\frac{A_e}{A_b} \tag{3.31}$$

where A_b is the cross section area of the lower part of the separator defined by equation 3.27 and α_{in} is the oil volume fraction of the inlet stream. The component mass balance gives the oil volume fraction in the top outlet:

$$\alpha_t = \frac{1}{q_t}\left[\alpha_{in}\ q_{in} - \alpha_b\ q_b\right] \tag{3.32}$$

Where q_{in}, q_t and q_b are the volumetric flow rate at the inlet and top and bottom outlet, respectively.

3.3.6 Summary of Gravity Separator Model

The model described above provides the necessary equations to estimate the oil volume fractions in the outlets (eq. 3.31 & 3.32) given the inlet composition, the flow rate and the flow split of the gravity separator. A prerequisite is that the physical dimensions of the separator and the properties of the emulsion are known. The latter includes the densities of the pure phases, the average droplet size and a correlation between the viscosity and oil content of the emulsion.

The model is based on two independent plug flows flowing through the separator and exiting through two respective outlets. The oil droplets are pushed upwards by gravitational buoyancy forces and passes from the lower to the upper plug flow while an equal amount of water moves in the opposite direction. The vertical movement of the droplets is estimated under the assumption that all droplets have the same vertical velocity (i.e., uniform droplet size distribution).

3.4 Model Input

In order for the models to produce any output, they must be provided with a set of input properties. This includes fluid properties of the particular emulsion, the physical dimensions of the separators and empirical parameters to the models. An experimental setup with a swirl separator for oil-in-water emulsions has been constructed by van Campen

[18]. To validate the model, the fluid properties and the dimensions of this separator model are set equal to those used in these experiments.

There are no experimental data available for the two remaining separators (i.e., gravity- and water-in-oil swirl separator). Therefore, a set of dimensions has been made up for each separator. This allows us to investigate the characteristics of two hypothetical separators. It also makes it possible to do optimization of a separation system containing all three separators.

The oil volume fraction and flow rate of the inlet emulsion and the flow split of the separators are also considered as model input. These inputs are, however, not discussed in this chapter as the simulations are run for a range of these values.

3.4.1 Fluid Properties

The fluid properties are input parameters to the separator models and are chosen in an attempt to reconstruct the experiments performed by van Campen [18]. The water phase is brine made of tap water and sodium chloride (NaCl). The oil phase is a *refined mineral oil blended with zinc free additives* [18]. The densities and viscosities of the two phases are presented in Table 3.1. The viscosity of the brine is not specified in the thesis by van Campen [18], but the viscosity of pure water at 20 °C is assumed to be accurate enough for this type of crude models.

The models require the viscosity of the emulsion as a function of the oil cut. The viscosity is expressed by a third order polynomial function

Table 3.1: Properties of the oil and brine used as input for the separator models.

Liquid	Density $[kg/m^3]$	Viscosity $[mPa \cdot s]$
Oil	881	8.8
Brine	1064	1.0

(eq. 2.7), which is fitted to experimentally measured values by van Campen [18]. The phase inversion point of this particular emulsion is measured to be at the oil volume fraction of 0.66. This means that the viscosity function must be divided into two different regions with different polynomial coefficients. One for oil-in-water emulsions ($\alpha \leq 0.66$) and one for water-in-oil emulsions ($\alpha > 0.66$).

The polynomial function for the oil-in-water emulsion is presented alongside the experimentally measured values in Figure 3.12. It shows the relative viscosity (normalized by the viscosity of water) as a function of the oil volume fraction in the emulsion. The viscosity is measured for the LPO stream, while the stated oil volume fraction is for the inlet stream. Since the oil volume fraction is greater at the LPO than at the inlet, the measured viscosity is higher than the actual viscosity at the inlet. However, the experiment was run at a low flow rate with a weak swirl element (i.e., low swirl number) so the degree of separation is expected to be low. The compositions at the outlets are not specified for this experiment, but similar experiments show that almost no separation occurs at $\alpha < 0.1$ and $\alpha > 0.6$. In the region between (i.e., $0.1 \leq \alpha \leq 0.6$), the experimental measured viscosities show little change, which suggests that there is no significant increase in the degree of separation. As a result, the assumption $\alpha_{in} \approx \alpha_{LPO}$ is to some extent

expected to be accurate for this experiment. However, the viscosity is expected to be overestimated to a certain degree in the region $0.1 \leq \alpha \leq 0.6$.

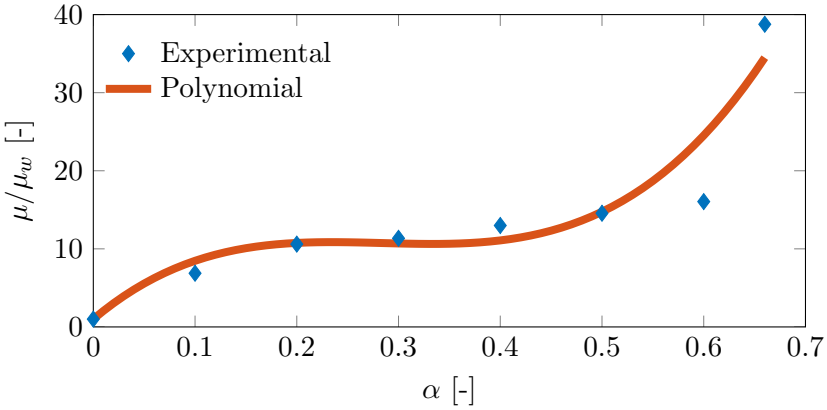

Figure 3.12: Relative viscosity of the oil-in-water emulsion, μ, as a function of the oil volume fraction, α. The polynomial is used as a model input and is fitted to the experimentally measured values [18]. The viscosity is measured at the LPO of the oil-in-water swirl separator with the corresponding inlet oil cut listed on the x-axis.

The corresponding polynomial function for the water-in-oil emulsion is presented alongside the experimental measure values in Figure 3.13. The experimental procedure for the viscosity measurements is the same as for the oil-in-water emulsion. The separator used in the experiment is designed for oil-in-water emulsions. This means that the degree of separation is expected to be even lower for water-in-oil emulsions so the assumption $\alpha_{in} \approx \alpha_{LPO}$ is expected to be stronger for this case.

The polynomial coefficients for the two viscosity equations are listed in Table 3.2. These are used as input variables for the separator models.

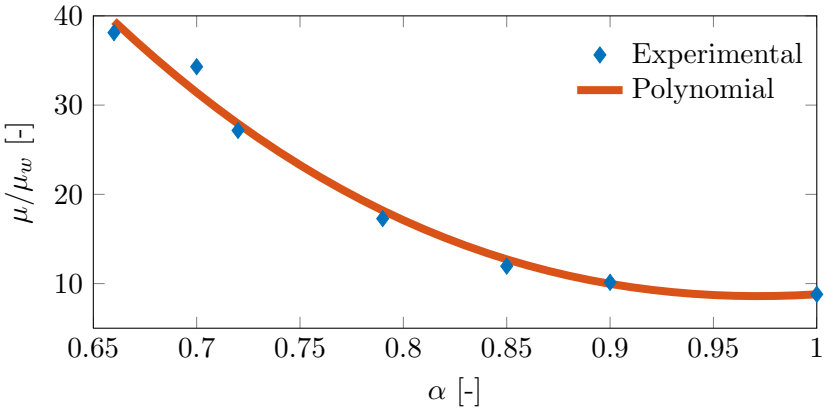

Figure 3.13: Relative viscosity of the water-in-oil emulsion, μ, as a function of the oil volume fraction, α. The polynomial is used as a model input and is fitted to the experimentally measured values [18].

Note that the fluid properties presented in this section are chosen for the sake of validating the oil-in-water swirl separator model with experimental data. The properties of well fluids found at different oil fields vary significantly and the input to the model must be assessed for each individual case.

Table 3.2: Fitted values for the coefficients in the polynomial for the viscosity of the emulsion $\mu = \mu_c \left(1 + a\varphi + b\varphi^2 + c\varphi^3\right)$. Where μ_c is the viscosity of the continuous phase and φ is the volume fraction of the dispersed phase.

Emulsion	Range in α [-]	a [-]	b [-]	c [-]
Oil-in-water	$0 - 0.66$	110	-400	470
Water-in-oil	$0.66 - 1$	-1.6	27	23

3.4.2 Swirl Separator for Continuous Water Phase

The necessary input to the oil-in-water swirl separator are the separator dimensions, average droplet size and three empirical parameters. The input variables are set on the basis of the experimental work conducted by van Campen [18].

Separator Dimensions

The physical dimensions of the oil-in-water swirl separator are set to represent the lab-separator by van Campen [18]. During the experiments, some of the dimensions are modified by changing out parts. This includes the distance from the swirl element to the inner pipe, L, and the radius of the inner pipe, R_i. The changes in these dimensions are relatively small and show no significant effect of the separation efficiency. As a result, only the nominal values are considered in this thesis. The dimensions are listed in Table 3.3.

In the experiments conducted by van Campen [18], three different swirl elements are used. The swirl elements have different strengths, which means that they generate different tangential velocities given the same flow rate. The stronger the swirl element is, the greater the associated swirl number, Ω, is. The swirl number is defined in equation 3.5. The *large* swirl element has a diameter that is greater than the diameter of the of the separator. To connect it with the separator, a tapering section where the diameter is gradually reduced is located between the swirl element and the separator tube. The conservation of angular momentum means that the tangential velocity increases as the

Table 3.3: Physical dimensions of the oil-in-water swirl separator. Three different swirl elements (i.e., large, strong & weak) are used in the separator. This results in three different swirl numbers.

Length	Outer pipe	Inner pipe	Swirl number
L [m]	R [m]	R_i [m]	Ω [-], large/strong/weak
1.7	0.05	0.025	7.0/5.0/3.5

diameter decreases. The swirl number for the three swirl elements are measured experimentally and presented in Table 3.3. Unless otherwise is indicated, the *large* swirl element is used.

Average Droplet Size

The average (i.e., volume average) droplet size is given by an empirical correlation to the maximum tangential velocity. The domain is divided into two intervals and two linear functions are fitted to experimentally measured values. The average droplet diameter, D_d, is then given by:

$$D_d(v_\theta^{max}) = \begin{cases} (-107 \cdot v_\theta^{max} + 600) \cdot 10^{-6}, & v_\theta^{max} \leq 4.45 \\ (-8 \cdot v_\theta^{max} + 160) \cdot 10^{-6}, & v_\theta^{max} > 4.45 \end{cases} \tag{3.33}$$

The empirical correlation is compared to experimentally measured values in Figure 3.14. The experimental values show a clear correlation between the average droplet size and the tangential velocity. The fact that the measured values are relatively coherent for the different swirl elements (i.e., different swirl numbers) indicates that droplet break-up is mainly a function of the tangential velocity. This is an essential assumption for equation 3.33 (as discussed in Chapter 3.1.5). Note that the error bars in Figure 3.14 represent the standard deviation of the droplet size distribution and *not* the measurement error.

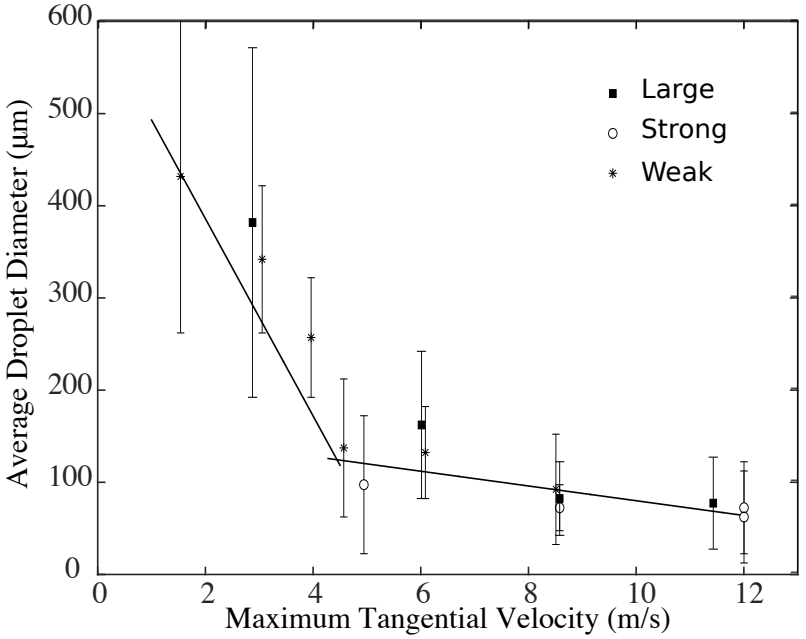

Figure 3.14: The average droplet diameter, D_d, versus the maximum tangential velocity, v_θ^{max}. Error bars indicate the standard deviation in the droplet size distribution. Solid lines represent equation 3.33. Measurements are done for the three different swirl elements. Data adapted from van Campen [18].

Another assumption associated with equation 3.33 is that the average droplet size in the inlet emulsion, upstream of the swirl element, is greater than the droplet size given by the equation. This assumption comes from the fact that the swirl element mainly causes droplet break-up and not droplet coalescence. The droplet size of the inlet fluid will typically be low if there is another separator located just upstream of the particular separator. The validity of the assumption must therefore be questioned if the separator is down stream of another separator and the swirl number and flow rate are low.

Empirical Parameters

Three parameters are found empirically and are listed in Table 3.4. These are:

- The radius of the inner core with a solid body rotation (i.e., R_c in eq. 3.4).
- The damping coefficient representing loss of momentum (i.e., C_{decay} eq. 3.6).
- The re-entrainment coefficient (i.e., $k_{re\text{-}en}$ in eq. 3.15).

The radius of the inner core, modeled with a solid body rotation, is set to 25% of the separator radius, R (i.e., $R_c/R = 0.25$). This is a typical magnitude of the parameter reported by Dirkzwager [5] and it shows good agreement with the experimentally measured tangential velocity profiles [18]. The experimental data show some variation in R_c for different conditions (e.g., flow split, swirl number, etc.) with the measured values ranging from 20% and 30% of R [18]. However, the assumption that R_c is constant seems to be within the accuracy expected from this type of model.

The damping coefficient, C_{decay}, is reported to have been determined experimentally to be 0.04 [5, 16]. This value is a rough approximation as the decaying factor (exponential factor in eq. 3.6) generally decreases for greater swirl numbers [5] and probably depends on the viscosity of the emulsion.

The proportionality constant, $k_{re\text{-}en}$, for the re-entrainment rate was determined by fitting the model to experimental data provided by van Campen [18]. The fitting was performed at a flow rate of $10\,\mathrm{m^3\,h^{-1}}$

Table 3.4: Empirical parameters for the oil-in-water swirl separator. The parameters are used in equation 3.4, 3.6 & 3.15, respectively.

R_c/R [-]	C_{decay} [-]	$k_{re\text{-}en}$ [m^2]
0.25	0.04	$2 \cdot 10^{-4}$

because this is close to the flow rates the separator is optimized for (see Chapter 4 for optimization procedure). The fitting procedure is described in Appendix D. $k_{re\text{-}en}$ was determined to be $2 \cdot 10^{-4}$ m^2.

3.4.3 Swirl Separator for Continuous Oil Phase

The input to the water-in-oil swirl separator model is set to represent a hypothetical separator with similar characteristics as the water-in-oil separator defined in Chapter 3.4.2. The required input variables are the same for both swirl separator models and include the separator dimensions, the average droplet size and three additional model parameters.

Separator Dimensions

The physical dimensions of the water-in-oil swirl separator are set equal to those of the oil-in-water swirl separator except for the pickup tube, which is made wider (see Table 3.5). The radius is increased because the separator is designed for oil continuous emulsions, which means that it is expected to handle higher oil cuts. The LPO flow rate is therefore expected to be greater compared to the HPO flow rate. The relative cross section area of the pickup tube to the outer pipe is 0.73, compared to 0.15 for the oil-in-water swirl separator.

Table 3.5: Physical dimensions of the the water-in-oil swirl separator. Three different swirl elements (i.e., large, strong & weak) are used in the separator. This results in three different swirl numbers.

Length	Outer pipe	Inner pipe	Swirl number
L [m]	R [m]	R_i [m]	Ω [-], large/strong/weak
1.7	0.05	0.043	7.0/5.0/3.5

The physical dimensions of the separator are set as they are due to lack of experimental data. The model has been verified with the experimental data assuming minimum differences to the oil-in-water separator. Therefore, it is desirable to keep the dimensions of the two swirl separators as similar as possible.

Average Droplet Size

The correlation between the average droplet size and the maximum tangential velocity is assumed to be independent of which phase is continuous and which phase is dispersed. This assumption is made due to lack of experimental data. However, the interfacial tension is an important factor in determining the droplet stability [4, 6]. The interracial tension is dependent only on the properties of the two liquids in the emulsion, and not on which one is continuous and which one is dispersed. There are other factors (e.g., viscosity, densities, etc. [6]) that will affect the average droplet size, but these are neglected; so, the average droplet size is assumed to be given by equation 3.33.

Empirical Parameters

The empirical parameters for the water-in-oil swirl separator are set equal to those of the oil-in-water swirl separator (see Table 3.4). The parameters are already assumed to be independent of the oil cut in the region of continuous water phase, see Chapter 3.4.2. As the fluid properties (e.g., densities, viscosity, etc.) are varying in this region, adding the region of continuous oil phase will simply increase the range of the assumption, but will not change it. E.g., the damping coefficient, C_{decay}, on the swirl flow is expected to increase for more viscous emulsions as the shear stress is proportional to the viscosity. However, the damping coefficient is assumed constant (i.e., independent on the viscosity) for oil-in-water emulsions, even though the viscosity is varying. Hence, although the viscosity is generally expected to be higher for water-in-oil emulsions, the assumption is not violated.

A more complex model for the loss of angular momentum would improve the accuracy of the separator model, but that kind of complexity is not desired for the models developed in this thesis. The same applies for the two other empirical parameters (i.e., R_c & $k_{re\text{-}en}$) and their associated equations.

3.4.4 Horizontal Gravity Separator

The inputs to the gravity separator model are the physical dimensions of the separator and the average droplet size (Table 3.6). The inputs are set to model a hypothetical separator that is meant to do an initial bulk separation of an emulsion before it is further processed by the two swirl separators.

Table 3.6: Input to horizontal gravity separator.

Length L [m]	Outer pipe R [m]	Weir height H_w [m]	Droplet diameter D_d [μm]
7	1.7	2.55	120

The average droplet diameter is assumed to be 120 µm. This assumption is made in view of the lack of appropriate empirical or theoretical correlations. In order to improve the model, measurements of the droplet size or a method for predicting it is needed. Nevertheless, it is assumed that the model gives a reasonable tradeoff between the flow split and the purity of the product streams. This will allow us to do optimization of the swirl separators in the combined separation system described below.

3.5 Combined Separation System

A hypothetical separation system is created to study how the separators can work together to separate the incoming emulsion into an oil-rich product and a water-rich product. The system contains the three separators:

- Gravity separator:
  - Horizontal gravity separator.
  - Defined in Chapter 3.3 with the input parameters presented in Chapter 3.4.4.
- Dewaterer:
  - Swirl separator for continuous oil phase.

  - Defined in Chapter 3.2 with the input parameters presented in Chapter 3.4.3.

- Deoiler:
  - Swirl separator for continuous water phase.
  - Defined in Chapter 3.1 with the input parameters presented in Chapter 3.4.2.

The flow diagram for the separation system is presented in Figure 3.15. The gravity separator does a bulk separation while the dewaterer and deoiler purifies the water-rich and the-oil rich products, respectively.

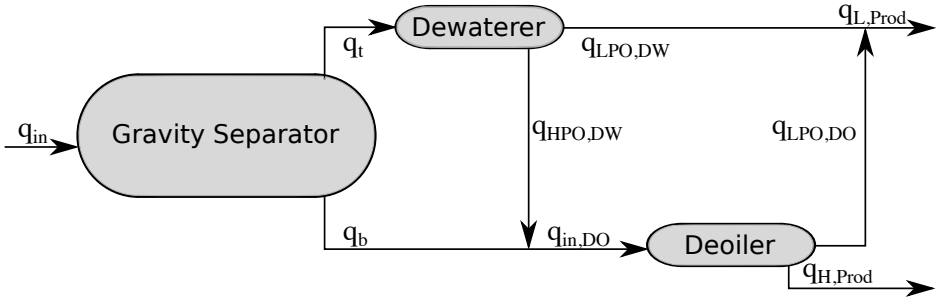

Figure 3.15: Flow diagram for the separation system consisting of the three modeled separators. The *dewaterer* is a swirl separator designed for a continuous oil phase, while the *deoiler* is a swirl separator designed for a continuous water phase.

4 Optimization Procedure

The separation system described in Chapter 3.5 has been optimized for the purity of oil-rich product with a constraint on the purity of the water-rich product. The considered inlet conditions, the objective function and the optimization procedure are described in this chapter and the results are presented in Chapter 5.4.

4.1 Inlet Conditions

The optimization has been performed for the inlet conditions that give the best separation performance. Since the separation system considered in this thesis is a hypothetical process, there is no particular region of inlet conditions that needs to be optimized. The inlet conditions have therefore been chosen on the basis of doing a meaningful optimization and are listed in Table 4.1. If the inlet conditions are set to values where each individual separator has a very poor performance, the optimal flow splits of the dewaterer and deoiler will be *one* and *zero*, respectively. That is, other flow splits will result in the swirl separators doing more mixing than separation.

The oil-in-water swirl separator (deoiler) has a maximum in the separation efficiency for inlet flow rates in the region of $10\,\mathrm{m^3\,h^{-1}}$ by use of the large swirl element (this is found in Chapter 5.2). The model identifies the absolute maximum at $q_{in}^{DO} = 8\,\mathrm{m^3\,h^{-1}}$, but no experimental data are available for flow rates lower than $10\,\mathrm{m^3\,h^{-1}}$ so it is desirable to keep the flow rate close to this value. The same behavior is found for the dewaterer by simulations (Chapter 5.1). The nominal inlet flow rate to the separation system is therefore set to $20\,\mathrm{m^3\,h^{-1}}$. This will result

Table 4.1: Nominal inlet conditions and swirl elements included in the optimization process.

α_{in} [-]	q_{in} [$m^3\,h^{-1}$]	Swirl Element Deoiler	Swirl Element Dewaterer
0.4	20	*large*	*large*

in the inlet flow rate to each of the swirl separators being in the region of $10\,m^3\,h^{-1}$, or at least the optimizer has the possibility to make it so.

The gravity separator model is only valid for feed flows that are oil-in-water emulsions. Since the emulsion considered in this work has its phase inversion point at $\alpha = 0.66$, the inlet oil cut is kept lower than 0.6. The deoiler and dewaterer are equally sized so they are designed to handle similar amounts of liquid. The separation system will therefore not perform optimally for too low values of the feed oil cut. Based on this, the nominal inlet oil cut is set to 0.4.

4.2 Objective Function

There are many possible objective functions for the separation system. The ideal objective function depends on what happens to the products downstream of the system. The product streams might be further processed and in that case the equipment downstream of the separation system can have specifications that will affect the optimal operating point.

The objective for the optimizer used in this thesis is to maximize the oil cut in the oil-rich product ($\alpha_{L,Prod}$), while keeping the oil cut in the water-rich phase ($\alpha_{H,Prod}$) less than some constraint (eq. 4.1). The

constraint on the water-rich product ($\alpha^{max}_{H,Prod}$) can be a specification on the water quality required for reinjection or discharge. The objective function takes the quality of the product streams into account, but it does not consider the recovery of oil (dilute efficiency, eq. 2.10). It is, however, assumed that the constraint on the water-rich product is low enough for the loss of oil to this stream to be negligible.

$$\begin{aligned} &\max \alpha_{L,Prod} \\ &\text{subject to: } \alpha_{H,Prod} \leq \alpha^{max}_{H,Prod} \end{aligned} \tag{4.1}$$

The regulations set by the Petroleum Safety Authority Norway [13] states that the oil content in produced water for discharge should be less than $30\,\mathrm{mg\,L^{-1}}$ (i.e., ≈ 30 ppm). This would therefore be a reasonable value for $\alpha^{max}_{H,Prod}$. However, the separation system modeled in this thesis has a relatively low separation performance and the constraint would be impossible to reach without changing the design of the separators. It is desirable to use the model of the existing separator by van Campen [18], because it can be verified for these dimensions (see Chapter 5.1.1). As a consequence, the maximum allowed oil content in the water-rich product is set to 3%.

$$\alpha^{max}_{H,Prod} = 0.03$$

This constraint is significantly higher than what is expected to be the case for a real industrial separation system. However, the constraint can be lowered to any desirable value if the performance of the separation system is improved.

4.3 Execution of the Optimization Procedure

The objective function is maximized by use of the MATLAB optimizer *fmincon* with the *interior point* algorithm. *Fmincon* finds the minimum

of a given multivariable cost function with nonlinear constraints [8]. The objective function (eq. 4.1) is rewritten to become a minimization problem (eq. 4.2) with respect to the flow splits of the separators (eq. 4.3).

$$\begin{aligned} &\min_{\vec{FS}} \left(1 - \alpha_{L,Prod}\right) \\ &\text{subject to: } \alpha_{H,Prod} \leq \alpha_{H,Prod}^{max} \end{aligned} \tag{4.2}$$

$$\vec{FS} = \begin{bmatrix} FS_G \\ FS_{DW} \\ DS_{DO} \end{bmatrix} \tag{4.3}$$

The subscripts G, DW and DO represent the gravity separator, dewaterer and deoiler, respectively.

The model of the separation system (Chapter 3.5) is a set of equality and inequality constraints. The inequality constraints concern the oil volume fractions and the flow rates. The oil volume fractions are, by definition, constrained between *zero* and *one*. The flow rates are set to be positive, which leads to the flow splits being constrained between *zero* and *one* as the liquid is assumed to be incompressible. There are three additional inequality constraints, which are listed in Table 4.2. The oil cuts in the feed flows to each of the swirl separators are constrained in order to have the desirable continuous phase. As the actual separation performance is minimized at the point of phase inversion (see Chapter 5.1.1), and the model is invalid close to this point, the constraints are shifted to each side (of $\alpha = 0.66$).

The MATLAB script used to run the optimization procedure are presented in Appendix C.4.

Table 4.2: Inequality constraints related to the objective of the optimizer. These constraints are chosen for this optimization process while the remaining constraints are given by the models and must always be satisfied (independently of the chosen objective function).

Variable	min	max
α_t [-]	0.7	1
$\alpha_{in,DO}$ [-]	0	0.6
$\alpha_{H,Prod}$ [-]	0	0.03

5 Results and Discussion

The simulation and optimization results are presented and interpreted in this chapter. Each model is studied separately in Chapter 5.1-5.3, while the optimal operational points of the separation system at different inlet conditions are presented and discussed in Chapter 5.4.

5.1 Swirl Separator for Oil-in-Water Emulsions

The swirl separator for continuous water phase has been examined to find the characteristics of the separator and to verify the model. The model is described in Chapter 3.1 and the input values are presented in Chapter 3.4.2.

The model shows a good fit with experimental measurements [18], but some disagreements are found. The model output at different operational conditions are compared to the corresponding experimental values in Chapter 5.1.1.

The modeled separation performance is sensitive to changes in the flow rate. The separation performance can be maximized by finding the flow rate where there is an optimal balance between the centrifugal forces (i.e., swirl intensity) and the droplet break-up and residence time (Chapter 5.1.2). The flow split affects the separation performance by directing the impurities into the desirable outlet stream. For a given set of inlet conditions there can be found a flow split that maximizes the dispersed efficiency (Chapter 5.1.3).

5.1.1 Comparison to Experimental Data

The aim for this section is to verify the model by comparing the simulated separation performance to experimental values. The focus is on whether or not the model is coherent with the experiments, not on what characteristics this gives the separator. The experiments are performed by van Campen [18] and covers a range of flow rates, oil cuts, flow splits and swirl numbers.

The separation performance for different oil cuts in the feed is simulated and compared to the experimental values (see Figure 5.1). The experiment is performed with a flow rate of 10 $m^3\,h^{-1}$ with the large swirl element. The flow split is kept equal to the oil cut in the feed (i.e., $FS = \alpha_{in}$). The simulated and experimental values show good agreement for low values of α_{in}, but the accuracy of the model decreases for $\alpha_{in} \gtrsim 0.45$. The decrease in separation performance for high values of α_{in} is most likely caused by phase inversion [18], where a part of the liquid goes from an oil-in-water emulsion to a water-in-oil emulsion. Even though the modeled viscosity increases in this region (see Figure 3.12 for viscosity function), other effects of the phase inversion that might reduce the separation performance are not included in the model. The mismatch for high oil cuts in the feed is therefore to some extent expected. However, the separator is used as a deoiling unit and is therefore expected to handle emulsions with lower oil cuts. For this purpose, the simulated performance shows good agreement with the experimental values.

The experimental data presented in Figure 5.1 were used to tune the re-entrainment coefficient, $k_{re\text{-}en}$, in equation 3.15. This means that these

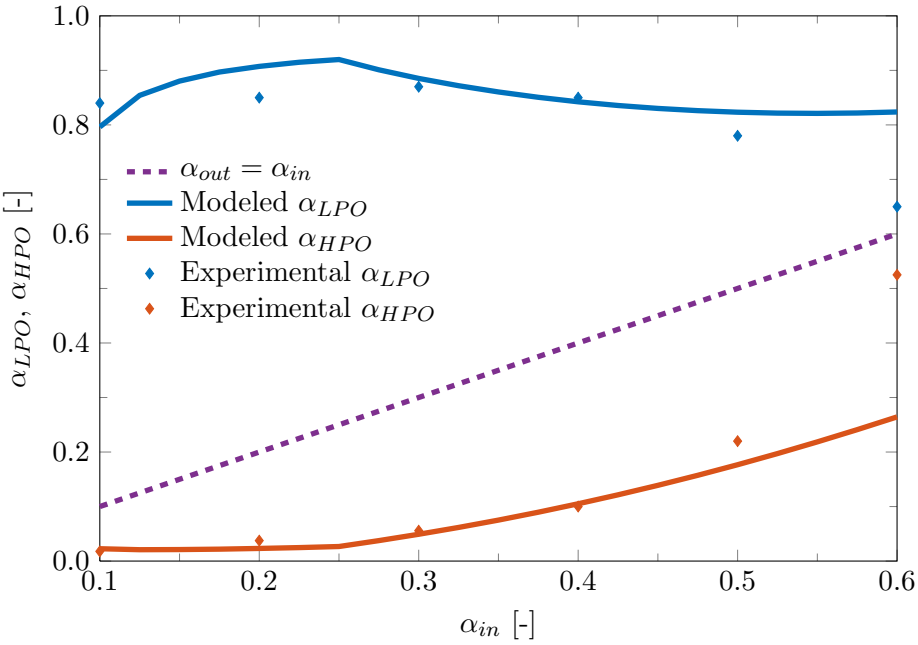

Figure 5.1: Oil volume fraction in the outlets versus the inlet. The large swirl element is used and the flow rate is 10 m^3/h. The flow split is set to $FS = \alpha_{in}$. The dashed line indicates the line of no separation. The experimental values are provided by van Campen [18]. Note that the experimental data are read from graphs and may contain some error.

data are inappropriate to use for model verification. That is, since the parameter is fitted to the experimental data, the fit is given and does not verify the model. However, if the same value of $k_{re\text{-}en}$ still shows good agreement with the experimental data when the operational conditions are changed, this would strongly indicate that the model makes good predictions. The procedure of determining $k_{re\text{-}en}$ is described in Appendix D.

The simulated and experimental separation performances are compared for different flow rates (see Figure 5.2). The experimental procedure is the same as in the case described above, but three different flow rates are examined. Note that the case with $q_{in} = 10\ \mathrm{m^3\,h^{-1}}$ is the same as in Figure 5.1. The simulated and experimental values are still relatively coherent. The agreement is good for low values of α_{in} and it decreases significantly as α_{in} approaches 0.6.

In contrast to the case with $q_{in} = 10\ \mathrm{m^3\,h^{-1}}$, the model overestimates the separation performance at $\alpha_{in} = 0.1$ for $q_{in} = 20$ and $30\,\mathrm{m^3\,h^{-1}}$. The simulated oil cut in the LPO is approximately twice the size of the experimental value. However, since the flow rate in the LPO is relatively low when $FS = 0.1$, the predicted oil volume fraction at this flow split is very sensitive to errors in the model. If we instead consider the dispersed efficiency of the separator, the error of the model at $\alpha_{in} = 0.1$ is less than 9% with $q_{in} = 30\ \mathrm{m^3\,h^{-1}}$ (see Appendix E). The dispersed efficiency for this case is shown in Figure 5.3. It is still clear that the model overestimates the separation performance, but the relative error becomes smaller. The inaccuracy of the model can therefore, perhaps, be considered acceptable depending on its application. If the aim is to estimate the oil cut in the LPO, this model is not suitable at very low values of α_{in} and $q_{in} = 30\,\mathrm{m^3\,h^{-1}}$.

Another observation that can be made from Figure 5.2 is that the model error is significantly higher for the flow rate of $30\ \mathrm{m^3\,h^{-1}}$. The model predicts a slight increase in the separation performance when the feed rate is increased from 20 to $30\ \mathrm{m^3\,h^{-1}}$. The experimental

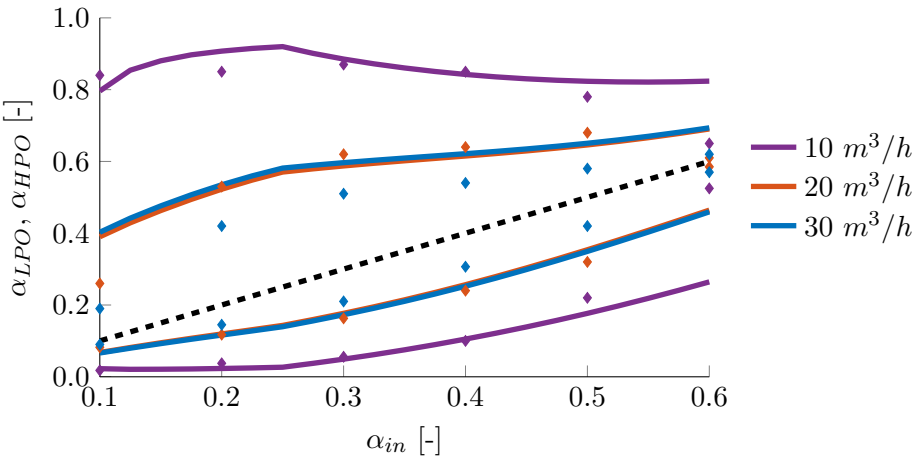

Figure 5.2: Oil volume fraction in the outlets versus the inlet for three different flow rates in the feed. The large swirl element is used and the flow split is set to $FS = \alpha_{in}$. The diamond markers represent the experimental values and the solid lines with the same colors represent the corresponding simulated values. The experimental values are provided by van Campen [18].

values do, on the other hand, show that the separation performance decreases. Increasing the feed rate increases the centrifugal buoyancy forces, but it also increases droplet break-up (i.e., reduces the average droplet size). The model predicts a local minimum in the separation performance with respect to the flow rate at $q_{in} \approx 18$ $\mathrm{m^3\,h^{-1}}$ (this is described in Chapter 5.1.2). This flow rate corresponds to the maximum tangential velocity where the empirical expression for the droplet size (eq. 3.33) switches from one region to another (i.e., at $v_\theta^{max} = 4.45$ $\mathrm{m\,s^{-1}}$). The local minimum is expected at this location as both the droplet size and the tangential velocity have positive effects on the separation. The tradeoff between these variables introduces a local minimum

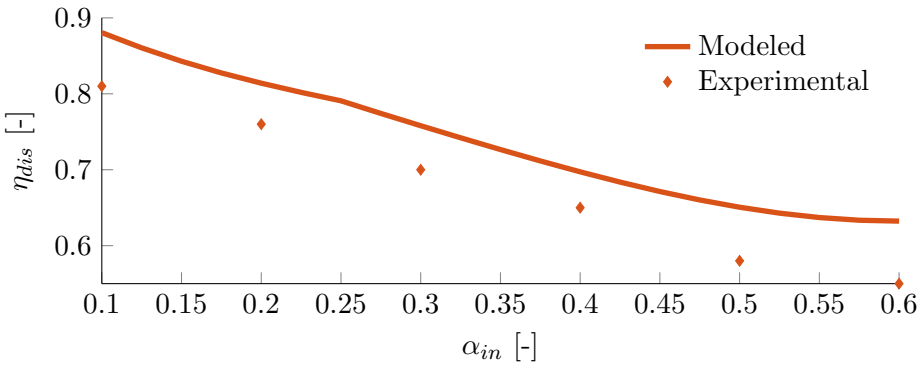

Figure 5.3: Dispersed efficiency versus inlet composition for $q_{in} = 30\ m^3/h$. The large swirl element is used and the flow split is set to $FS = \alpha_{in}$. The experimental values are provided by van Campen [18].

where the slope of the droplet size function changes (see Figure 3.14) as the product of the two variables ($v_\theta^{max} \cdot D_d$) has a minimum at this point.

The measured correlation between the droplet size and the tangential velocity also has a clear change in the slope so it is evident that a local minimum should occur also for the experimental case. However, the empirical expression (eq. 3.33) is fitted to values for all three of the swirl elements. If only the strong swirl element was considered, the kink in the function would occur in the region of $v_\theta^{max} \approx 7\ \mathrm{m\,s^{-1}}$, which corresponds to $q_{in} \approx 28\ \mathrm{m^3\,h^{-1}}$. The local minimum would then occur here. This seems likely given the experimental results in Figure 5.2, but experimental data at $q_{in} > 30\ \mathrm{m^3\,h^{-1}}$ is necessary to confirm or disprove the claim. If the statement is correct, the model would be improved by fitting the droplet size equation to the measured values for the *large* swirl element only. However, the average of the measurements is used as it is desirable to have a fixed model that is suitable for any swirl element.

Additionally, the fact that only four measurements are available for the large swirl element in Figure 3.14, would increase the uncertainty of the correlation.

The effect of the flow split on the separation efficiency is studied for three different oil volume fractions in the feed (i.e., $\alpha_{in} = 0.15$, 0.25 & 0.40), see Figure 5.4. The experiment is conducted with the *strong* swirl element and a flow rate of $56.5\,\mathrm{m^3\,h^{-1}}$. The simulated and experimental efficiencies show good agreement except for the case with $\alpha_{in} = 0.15$. This confirms the uncertainty of the model at low values of α_{in}. In this case the model underestimates the degree of separation, while it is overestimated for high flow rates in the case studied in Figure 5.2; this means that there is no obvious consistency in the mismatch of the model. The dependency of the separation efficiency on the flow split shows very similar trends for the simulated and experimental values. That is, the offset is almost independent of the flow split. This indicates that the modeled correlation between the efficiency and flow split is good.

These results reinforce the assumptions made in context of the re-entrainment rate as they mainly affect the separation efficiency as a function of the flow split (for description of these assumptions, see Chapter 3.1.7). An assumption that can be directly confirmed by the simulations is that the re-entrainment rate is low compared to the flow rate in the HPO (i.e., $|q_{re\text{-}en}/q_{HPO}| \ll 1$). For the simulations presented in Figure 5.2, $|q_{re\text{-}en}/q_{HPO}| < 0.12$ for all values of FS. The separator is expected to operate at flow splits less than 0.4; at least the optimal operational conditions estimated in Chapter 5.4 are in this region.

For these flow splits, $|q_{re\text{-}en}/q_{HPO}| < 0.03$ so the assumption can be considered valid.

Overall, the model shows good agreement with the experimental data. The model show satisfying result for the conditions:

- Inlet oil cuts (α_{in}) between 0.2 and 0.45.
- Flow rates (q_{in}) between 10 and 20 $\mathrm{m^3\,h^{-1}}$.
- All tested flow split (FS), i.e., between 0.15 and 0.6.

The accuracy of the model outside this region is varying and will in some cases be unreliable. This is important to take into account when using the model for any purpose (e.g., optimization). However, the model can do satisfactory predictions outside this region, but a certain degree of carefulness is recommended.

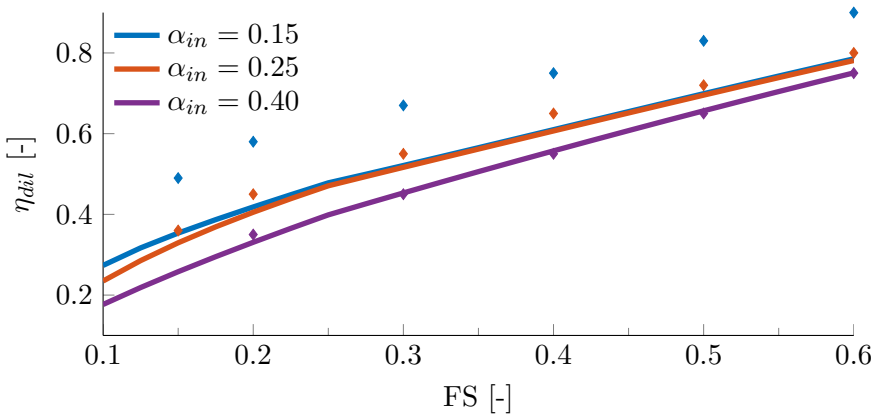

(a) Dilute efficiency.

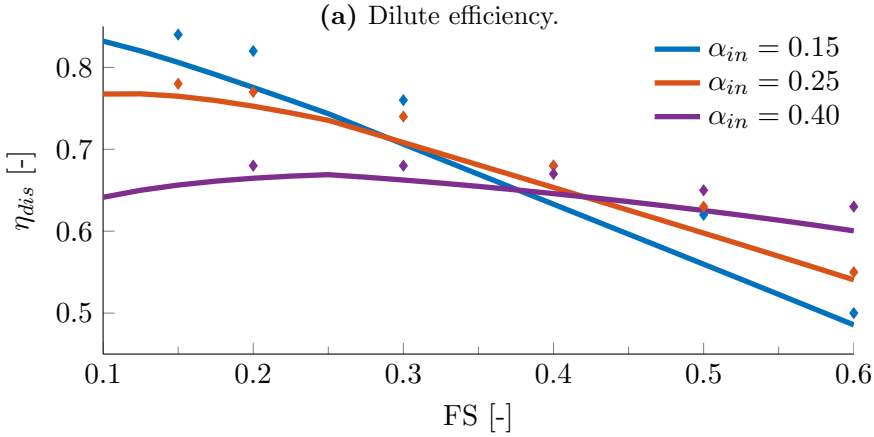

(b) Dispersed efficiency.

Figure 5.4: Efficiency versus flow split for three different oil cuts in the inlet, α_{in}. The experimental data [18] are represented by diamonds while the corresponding simulations are represented by solid lines with the same colors. The *strong* swirl element is used and the flow rate is 56.5 m^3/h. The dilute and dispersed efficiencies are defined in Chapter 2.5. Note that the experimental data are read from graphs and may contain some error.

5.1.2 Effect of the Flow Rate

The effect of the inlet flow rate on the separation efficiency of the model is studied for the *large* and the *strong* swirl element. The dispersed efficiency curve has two local maxima and one local minimum with respect to the flow rate, see Figure 5.5. This behavior is mainly influenced by the empirical droplet size correlation (eq. 3.33). The local minimum is located at the flow rate that corresponds to a maximum tangential velocity of $4.45\,\mathrm{m\,s^{-1}}$ because the slope of the droplet size correlation changes at this value. As the *large* swirl element corresponds to a greater swirl number than the *strong* swirl element, the local minimum occurs at a lower flow rate. This is an important consideration when doing design of a swirl separator.

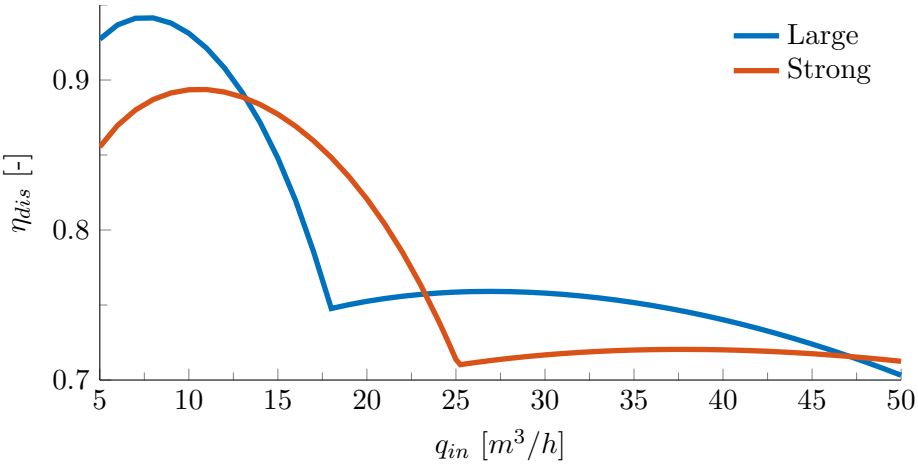

Figure 5.5: Dispersed efficiency (η_{dis}) versus flow rate (q_{in}). The swirl separator is simulated for two different swirl elements. The large swirl element has a greater swirl number than the strong swirl element. $FS = \alpha_{in} = 0.3$.

When doing optimization of a fixed design, the accuracy of the predicted local maxima is vital. The optimizer will try to push the inlet flow rate towards one of the maxima so the corresponding flow rate becomes an important property of the model. As discussed in Chapter 5.1.1, the model has a significant mismatch in the local minimum compared to the experimental data (for the large swirl element). This indicates that a corresponding mismatch could be present for the local maxima. The mismatch is most likely a result of the inaccuracy of the droplet size equation. The equation fits better to the data for the weak and strong swirl elements (see Figure 3.14) so the mismatch is assumed to be less for these cases.

An assumption made in Chapter 3.1.5 is that the droplet size upstream of the swirl element is greater than the size estimated by the droplet size equation (eq. 3.33). This assumption is generally satisfied for the experimental work considered in this thesis [18]. However, for an industrial separator where the droplets are exposed to more stress upstream of the swirl element, the assumption might be violated. The maximum separation efficiency is at $q_{in} \approx 8\,\mathrm{m^3\,h^{-1}}$ for the large swirl element (Figure 5.5). The estimated average droplet diameter at this flow rate is approximately 400 µm. This is relatively large and might exceed the initial droplet size for many processes, in which case the model will overestimate the separation efficiency. In order to include this in the model a correlation for the droplet size upstream of separator is necessary and this behavior will vary for different processes.

5.1.3 Effect of the Flow Split

The flow split can be manipulated to affect the quality of the product streams. This introduces a tradeoff between the purity of the LPO and HPO stream. The oil cut in the LPO and the water cut in the HPO for a simulation with $q_{in} = 56.5\,\mathrm{m^3\,h^{-1}}$, α_{in} =0.4 and the *strong* swirl element is presented in Figure 5.6. The purity of the HPO stream increases with the flow split while the purity of the LPO stream decreases. As a consequence of this tradeoff, the dispersed efficiency has a maximum at $FS \approx 0.25$ (see Figure 5.4). The dilute efficiency does, on the other hand, increase with the flow split for the entire domain. The optimal value of the flow split will thus depend on the objective of the separator.

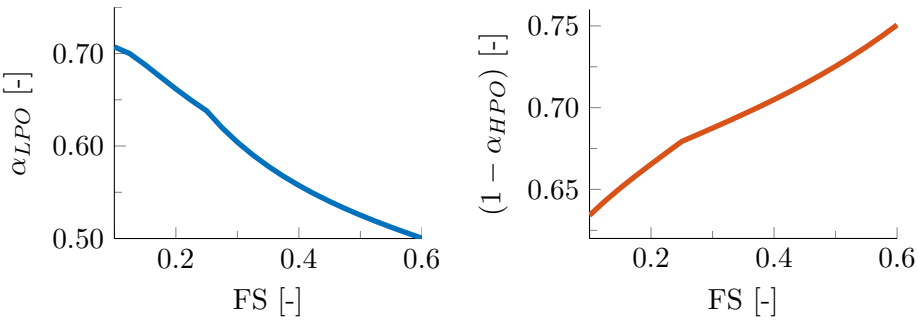

(a) Oil cut in LPO **(b)** Water cut in HPO

Figure 5.6: Purity of product streams versus flow split (FS). The *strong* swirl element is used. The inlet flow rate is 56.5 m^3/h and the inlet oil cut is 0.4. The corresponding efficiencies are presented in Figure 5.4.

5.2 Swirl Separator for Water-in-Oil Emulsions

The hypothetical swirl separator for continuous oil phase has been examined to find the characteristics of the separator. The model is described in Chapter 3.2 and the input values are presented in Chapter 3.4.3. There are no available experimental data to verify the model for the used separator dimensions (Table 3.5). However, a comparison to the experimental data provided by van Campen [18] is made in Appendix F by adjusting the separator dimensions to the ones used in his experiments. More experimental data are required to verify the model, but this comparison, along with the relative good fit of the oil-in-water swirl separator, is a good indication that the model has a certain degree of accuracy.

The separation performance predicted by the model is dependent on the operational conditions. These dependencies are important properties of the separator and are essential when doing optimization. The effect of the flow rate and flow split on the separation efficiency are discussed in Chapter 5.2.1 and 5.2.2, respectively.

5.2.1 Effect of the Flow Rate

The simulated performance of the water-in-oil swirl separator shows the same qualitative behavior as the oil-in-water swirl separator. The local extrema in the dispersed efficiency (η_{dis}) with respect to the flow rate (q_{in}) are located at the same values of q_{in} for the same swirl number, see Figure 5.7. This is a consequence of the same droplet size equation (eq. 3.33) and separator dimensions are being used for both models.

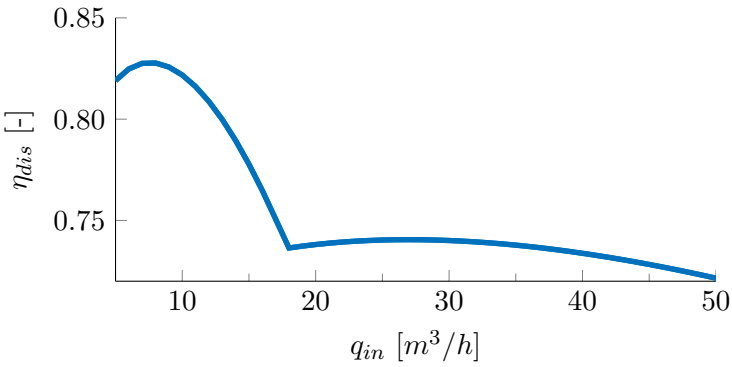

Figure 5.7: Dispersed efficiency (η_{dis}) versus flow rate (q_{in}) for the water-in-oil swirl separator. The large swirl element is used and $FS = \alpha_{in} = 0.8$.

5.2.2 Effect of the Flow Split

The modeled performance of the water-in-oil separator shows that there is a tradeoff between the purity at the LPO and the purity at HPO, see Figure 5.8. When the flow split increases, the quality of the LPO decreases and the quality of the HPO increases. This is a consequence of more of the unseparated emulsion being shifted from the HPO to the LPO. The tradeoff between the two product streams leads to a maximum in the dispersed efficiency at $FS \approx 0.87$, see Figure 5.9. The maximum dispersed efficiency is generally located at a flow split slightly greater than the inlet oil cut (in this case: $FS \approx 0.87 > \alpha_{in} = 0.8$). The oil volume fraction of the LPO is, on the other hand, quite low at this flow split. The optimal value of the flow split will thus depend on the objective of the separator.

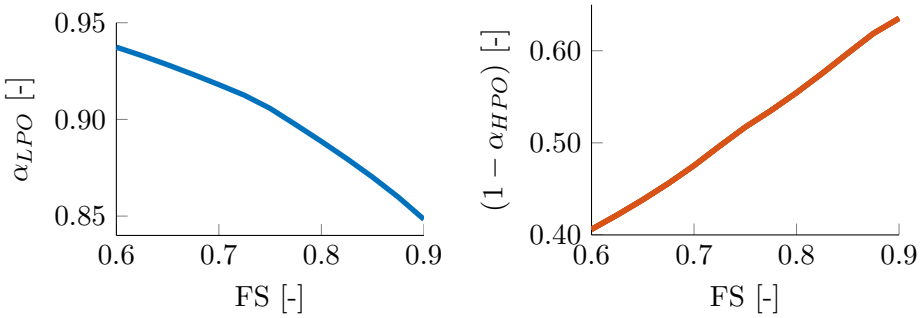

(a) Oil cut in LPO **(b)** Water cut in HPO

Figure 5.8: Purity of product streams versus flow split (FS) for the water-in-oil swirl separator. The *strong* swirl element is used. The inlet flow rate is 10 m^3/h and the inlet oil cut is 0.8.

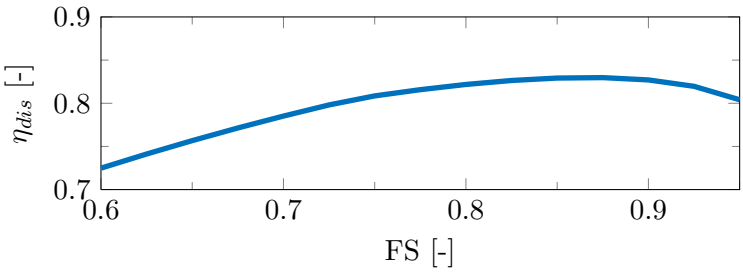

Figure 5.9: Dispersed efficiency versus flow split for the water-in-oil swirl separator. The conditions are the same as in Figure 5.8 (i.e., *large* swirl element, $q_{in} = 10\ m^3/h$ & $\alpha_{in} = 0.8$).

5.3 Gravity Separator

The hypothetical gravity separator is represented by a crude model, which is constructed in order to do optimization of the combined separation system (Chapter 3.5). The gravity separator allows the optimizer to manipulate the flow rate going into each of the swirl separators by adjusting the flow split. It is therefore important that the model predicts reasonable qualitative responses to changes in the flow split. It is, however, not expected that the model predicts accurate quantitative values for the purities of the product streams. That would require experimental data for fitting of parameters and model verification, and probably a more complex model. This work has not been performed in context of this thesis as the focus has been on the swirl separators.

The model is described in Chapter 3.3 and the input values are presented in Chapter 3.4.4.

5.3.1 Effect of the Flow Rate

The separation efficiency of the gravity separator decreases with the flow rate. The gravitational acceleration is, in contrast to the centrifugal acceleration of the swirl separators, constant so there is no enhancing effect of increasing the flow rate. There is, however, a reducing effect as the residence time decreases with the flow rate. The purities of the product streams for q_{in}= 20 & 25 $m^3\,h^{-1}$ are presented in Figure 5.10 and clearly show the reduced separation performance for the greater flow rate. This example is for an inlet oil cut of 0.4 and a varying flow split. Simulations ran at other conditions show the same trend.

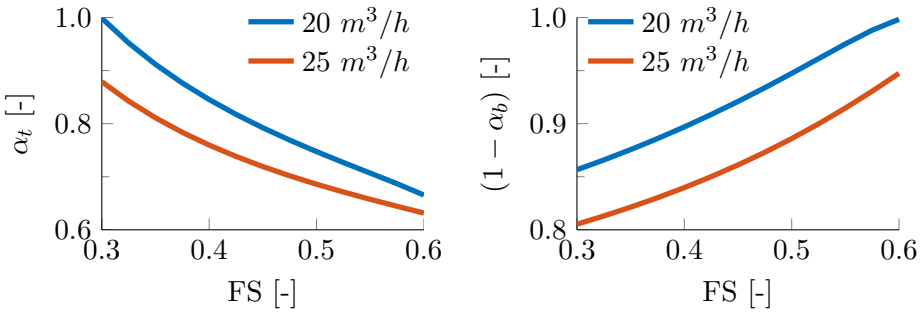

(a) Oil cut in top outlet **(b)** Water cut in bottom outlet

Figure 5.10: Purity of product streams versus flow split (FS) of the gravity separator. The inlet flow rates are 20 and 25 m^3/h and the inlet oil cut is 0.4.

5.3.2 Effect of the Flow Split

The simulations show that the purity of the top product decreases with the flow split while it increases for the bottom product (Figure 5.10). This means that taking out more product at the top leads to a reduced purity of the top product, and vice versa for the bottom product. This is an expected correlation and is caused by the unseparated emulsion being shifted from one product stream to the other. The tradeoff is an important factor in the optimization of the separation process as it sets the inlet conditions for the *dewaterer* and *deoiler* in the separation system (described in Chapter 3.5).

The simulated dispersed and dilute efficiencies are presented in Figure 5.11. It is obvious that the dilute efficiency increases with the flow split as more oil is taken out in the top outlet (for definitions of the efficiencies, see Chapter 2.5). The decreasing tendency of the dispersed

efficiency is a consequence of the oil cut in the feed being less than 50%. The concentration profile in the separator is assumed to be divided into three sections, i.e., a pure oil phase, an emulsion phase and a pure water phase (see Chapter 3.3.4). When the flow split is increased, some of the emulsion is shifted from the bottom to the top outlet stream. Because the emulsion phase is assumed to have the same oil cut as the feed, this leads to a negative correlation between η_{dis} and FS if $\alpha_{in} < 0.5$. That is, the emulsion phase contains more *impurities* if it is taken out in the top than the bottom. Consequently, there is a positive correlation between η_{dis} and FS if $\alpha_{in} > 0.5$.

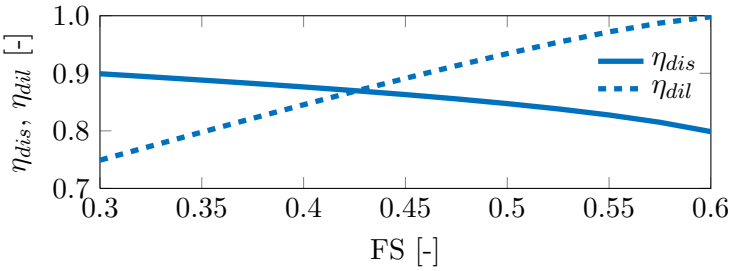

Figure 5.11: Efficiency versus flow split (FS) for the gravity separator. The conditions are $q_{in} = 20\ m^3/h$ & $\alpha_{in} = 0.4$. The corresponding purity of the product streams are shown in Figure 5.10.

5.4 Optimization

The separation system has been optimized with the procedure described in Chapter 4. The optimizer finds the combination of flow splits that leads to the greatest oil cut in the oil-rich product under the condition that the oil cut in the water-rich product does not exceed 3% (eq. 4.1). The

optimization procedure is based on the model for the separation system, which means that the inaccuracy in the model will propagate into the estimated optimum.

5.4.1 Effect of the Inlet Oil Cut

The effect of a change in the inlet oil cut on the optimal operational variables is presented in Figure 5.12 (the full overview is listed in Table G.1 in Appendix G). The optimal flow splits are estimated for $\alpha_{in} = 0.4$ and 0.5 with q_{in}=20 $\mathrm{m^3\,h^{-1}}$. The increasing oil cut in the feed leads to a reduced performance of the gravity separator due to the increased viscosity. To compensate for the increased amount of oil in the feed, the flow split of the gravity separator (FS_G^{opt}) increases from 0.33 to 0.40. This leads to a slight reduction in the quality of the top product. As a consequence of the relative increase in FS_G^{opt} being less than the relative increase in α_{in} and that the viscosity is increased, the purity of the bottom product is significantly reduced. As the oil cut in the top product is reduced, the flow split of the dewaterer (FS_{DW}^{opt}) decreases from 0.91 to 0.87. Similarly, the flow split of the deoiler (FS_{DW}^{opt}) increases from 0.15 to 0.27. The oil cut in the water-rich product is at the constraint of 3% for both cases. The oil cut in the oil-rich product is reduced from 0.94 to 0.92, mainly as a consequence of the reduced separation performance of the gravity separator.

Overall, the oil cut of the oil-rich product ($\alpha_{o,Prod}$) decreases slightly when the oil cut in the feed is increased. However, the flow rate of the oil-rich product increases from q_{in} = 8.1 to 10.5 $\mathrm{m^3\,h^{-1}}$ so the total amount of produced oil is improved. The recovery of oil (η_{dil}) increases

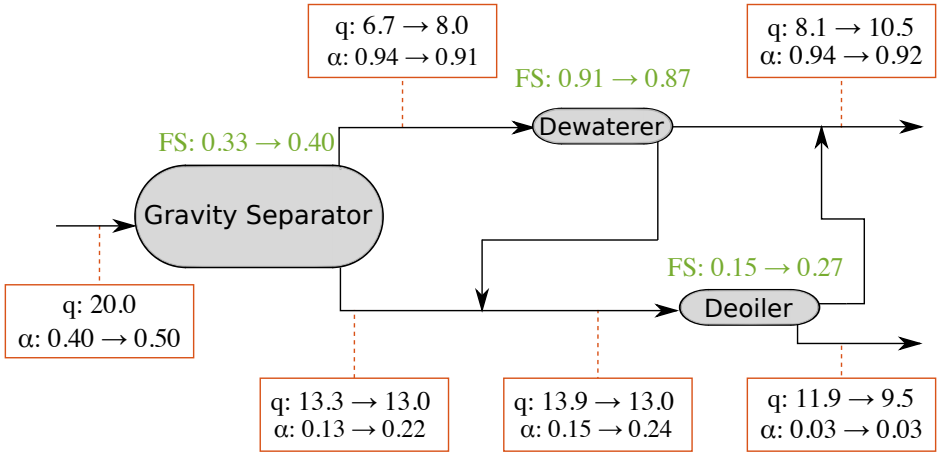

Figure 5.12: Optimal operations for change in inlet oil cut. The optimal flow splits (green) and estimated flow rates (q [$m^3\,h^{-1}$]) and oil volume fractions (α [-]) for some of the streams in the separation system. The oil cut in the inlet (α_{in}) is increased from 0.4 to 0.5 while the flow rate is kept constant at $20\,m^3\,h^{-1}$. The estimated values of the remaining streams are listed in Table G.1 in Appendix G.

from 96% to 97%. This is an essential observation because the loss of oil to the water-rich product is neglected from the objective function (eq. 4.1). The effect of the oil recovery on the optimum is not included as it is assumed to be close to 100% (see Chapter 4.2). The results confirm this assumption, especially considering that the constraint on the purity of the water-rich product would be even lower for a real industrial separation system (as discussed in Chapter 4.2), i.e., the oil recovery would be greater.

The accuracy of the model of the deoiler is likely to be relatively high for these conditions. The comparison to the experimental data shows that the model makes satisfying predictions for q_{in}= 10-20 $m^3\,h^{-1}$ and α_{in}= 0.1-0.2 with an exception at q_{in}= $20\,m^3\,h^{-1}$ and α_{in}= 0.1

(Figure 5.2). At the latter case, the model overestimates the separation performance, which introduces some uncertainty to the estimated optimum. The conditions are, however, quite close to the region where the model is considered to be sufficiently accurate so the optimum is assumed to be relatively reliable. The models for the gravity separator and the dewaterer are not compared to experimental data so the accuracies of these models are unknown.

The dependencies of the optimal flow splits on the inlet oil volume fraction are presented in Figure 5.13. The general trend is well represented by the case studied above. The flow split of the gravity separator increases due to the increased amount of oil in the feed. The increase in the viscosity of the inlet emulsion leads to more impurities in the inlet streams to the swirl separators, which result in an increase in the flow split of the deoiler and a decrease in the flow split of the dewaterer.

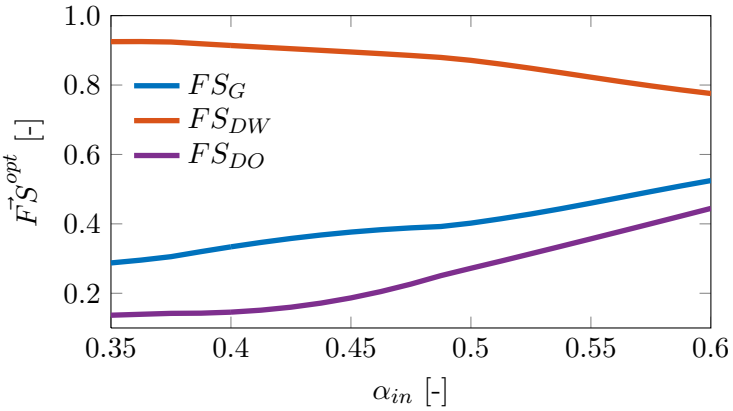

Figure 5.13: The optimal flow splits versus the inlet oil cut with $q_{in} = 20\,\mathrm{m^3\,h^{-1}}$. The subscripts correspond to the gravity separator (G), dewaterer (DW) and deoiler (DO).

The resulting oil volume fractions of the optimal flow splits, along with the corresponding values with fixed flow splits, are presented in Figure 5.14. The fixed flow splits are set as the optimal values at $\alpha_{in} = 0.4$ (i.e., $\vec{FS}^{fixed} = \vec{FS}^{opt}(\alpha_{in} = 0.4)$). It is evident that the optimal flow splits result in less water in the oil-rich product than the fixed flow splits for $\alpha_{in} < 0.4$ (Figure 5.14a). It is also apparent that the fixed flow splits lead to a violation of the constraint of the water-rich product for $\alpha_{in} > 0.4$ (Figure 5.14b). Overall, there is a clear advantage of using the optimized flow splits. Additionally, it can be observed that the relative small changes in $\vec{FS}^{opt}$ lead to significant consequences for the oil cuts in the product streams.

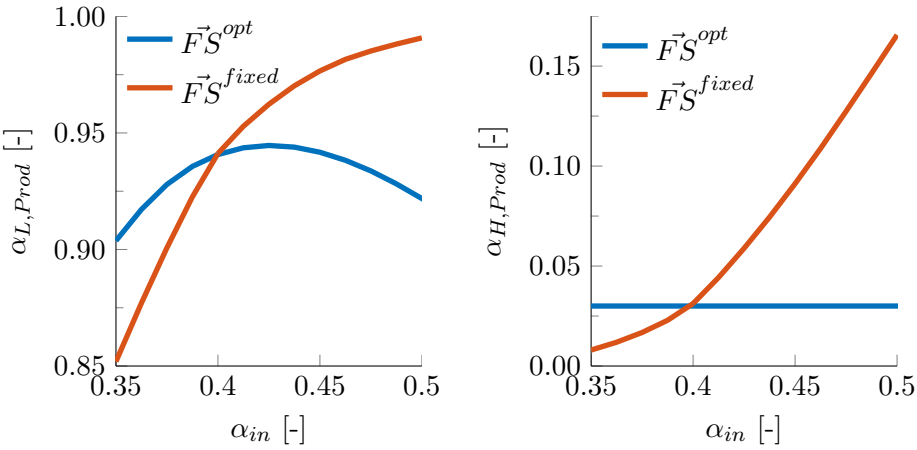

(a) Oil cut in oil-rich product. **(b)** Oil cut in water-rich product.

Figure 5.14: The oil cuts in the product streams versus the oil cut in the inlet stream of the separation system for $q_{in} = 20\,\mathrm{m^3\,h^{-1}}$. The product streams are estimated with the optimal flow splits ($\vec{FS}^{opt}$) presented in Figure 5.13 and with fixed flow splits ($\vec{FS}^{fixed}$). The latter are the optimal flow splits at $\alpha_{in} = 0.40$. The constraint of $\alpha_{H,Prod} \leq 0.03$ is violated when the fixed flow splits are used.

The oil volume fraction in the oil-rich product, which is the objective function of the optimizer, has a local maximum at $\alpha_{in} \approx 0.42$ (Figure 5.14a). This is a result of the design of the separation system and the value can be shifted to either side by changing the size of the deoiler and/or dewaterer. However, the aim of this thesis does not concern the design of the separation system and the inlet oil cut is considered a disturbance. Hence, this maximum has no significant meaning for the optimization process.

5.4.2 Effect of the Flow Rate

The effect on the optimal operational conditions for a change in the flow rate is presented in Figure 5.15. The flow rate of the inlet stream is increased from 20 to 25 $\mathrm{m^3\,h^{-1}}$ while the inlet oil volume fraction is kept constant at 0.4. The optimal flow split of the gravity separator increases from 0.33 to 0.46 even though the oil cut in the feed is fixed. Two aspects of the separation system can explain this observation:

1. The oil cut of the bottom product must be kept low in order for the deoiler to meet the constraint on the water-rich product (i.e., $\alpha_{H,Prod} \leq 0.03$).

2. The initial flow rate in the dewaterer is lower than the optimal value (i.e., 8 $\mathrm{m^3\,h^{-1}}$), while the initial flow rate in the deoiler is greater (see Chapter 5.1.2 & 5.2.1). It is therefore desirable to increase the flow rate to the dewaterer rather than the deoiler.

The increased flow split, combined with the reduced separation performance of the gravity separator at high flow rates, causes a significant reduction in the purity of the feed stream to the dewaterer. This leads to a decrease in the flow split of the dewaterer, but the reduction in the flow

split is considerably smaller than the reduction of the oil cut in the feed stream. This can, again, be explained by the desire to keep the flow rate and oil cut in the feed to the deoiler low. The slight increase in the flow rate through the deoiler causes the optimal flow split to increase from 0.15 to 0.17. The increase in the flow split is necessary to keep the oil cut in the water-rich product at 0.03.

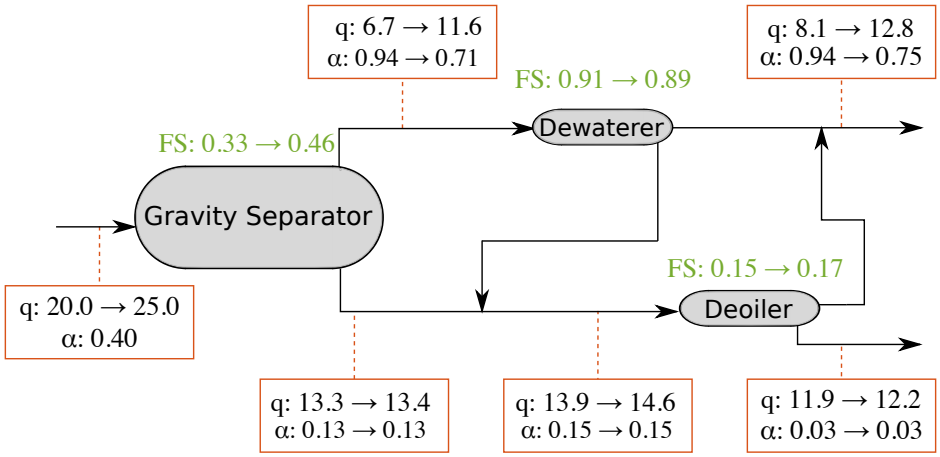

Figure 5.15: Optimal operations for change in the inlet flow rate. The optimal flow splits (green) and estimated flow rates (q [$m^3\,h^{-1}$]) and oil volume fractions (α [-]) for some of the streams in the separation system. The flow rate (q_{in}) is increased from 20.0 to 25.0 $m^3\,h^{-1}$ while the inlet oil cut is kept constant at 0.4. The estimated values of the remaining streams are listed in Table G.2 in Appendix G.

The oil volume fraction in the oil-rich product is reduced from 0.94 to 0.75. This reduction is an obvious consequence of the throughput being increased. The *bottleneck* in the system is the deoiler, which initially was operating with a greater throughput than desirable (i.e., $q_{in,DO}$ =

$13.9\,\mathrm{m^3\,h^{-1}} > 8\,\mathrm{m^3\,h^{-1}}$). The gravity separator and dewaterer do therefore have to "sacrifice" the quality of the light phase products in order to minimize the change in the feed to the deoiler. This makes the deoiler able to do the necessary separation to meet the constraint on the water-rich product, but the quality of the oil-rich product is significantly reduced.

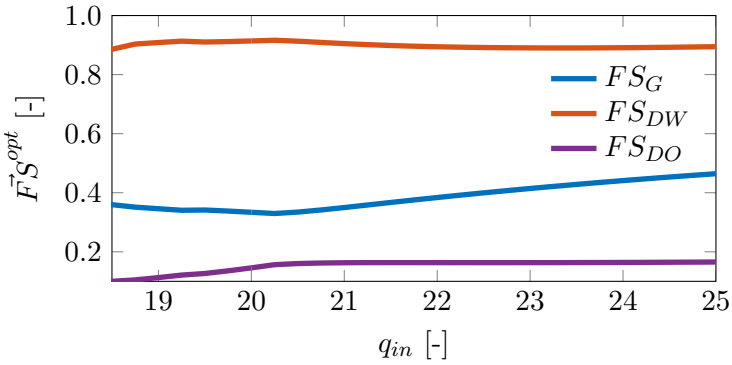

Figure 5.16: The optimal flow splits versus the inlet flow rate with α_{in}= 0.40.

The optimal flow splits versus the inlet flow rate for a fixed oil cut in the inlet, $\alpha_{in} = 0.40$, are presented in Figure 5.16. It can be observed that the sign of the slope of FS_G^{opt} changes at $q_{in} \approx 20\,\mathrm{m^3\,h^{-1}}$. This is probably caused by the fact that both the deoiler and the dewater have a local maximum in the separation efficiency at $q \approx 8\,\mathrm{m^3\,h^{-1}}$. In general, the flow rate to the deoiler is greater than to the dewaterer. Hence, there is a motivation to keep the flow rate to the dewaterer sufficiently high and the flow rate to the deoiler sufficiently low. The former effect dominates when q_{in} is low, while the latter dominates when q_{in} is large. In the region in between (i.e., $q_{in} \approx 20\,\mathrm{m^3\,h^{-1}}$), the outlet flow rates of the gravity separator have less importance and FS_G^{opt} is more affected by the desire to get optimal oil cuts in the outlet streams.

The resulting oil volume fractions of the product streams are presented in Figure 5.17. The optimal flow splits keep the oil cut of the water-rich product at the constraint of 0.03. The oil cut in the oil-rich product decreases significantly with the flow rate, which is a natural consequence of the residence time of the liquid in the separation system being reduced. Again, it can be seen that there is a clear advantage of optimizing the system as the fixed flow splits either reduce the quality of the oil-rich product or violate the constraint on the water-rich product.

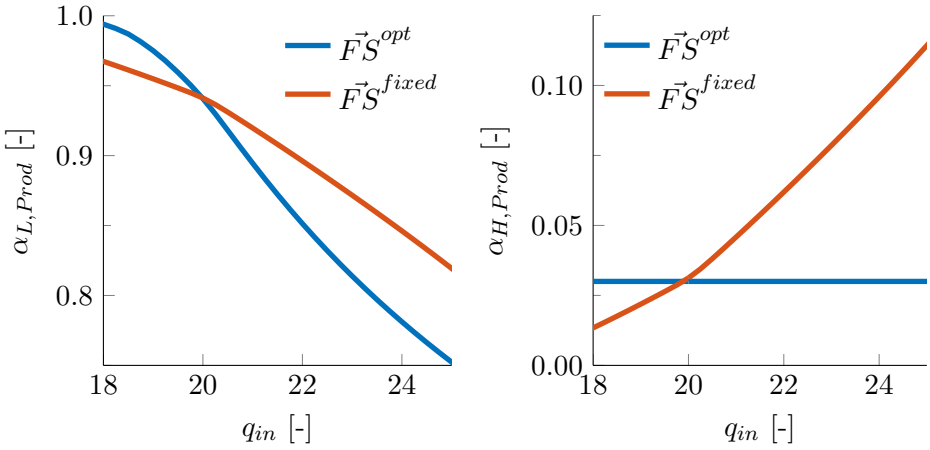

(a) Oil cut in oil-rich product. **(b)** Oil cut in water-rich product.

Figure 5.17: The oil cuts in the product streams versus the flow rate of the inlet stream for $\alpha_{in} = 0.40$. The product streams are estimated with the optimal flow splits ($\vec{FS}^{opt}$) presented in Figure 5.16 and with fixed flow splits ($\vec{FS}^{fixed}$). The latter are the optimal flow splits at $q_{in} = 20\,\mathrm{m^3\,h^{-1}}$. The constraint of $\alpha_{H,Prod} \leq 0.03$ is violated when the fixed flow splits are used.

6 Conclusion

A separation system for oil-water separation has been studied in this thesis. The system consists of a gravity separator for the bulk separation of the oil and the water into an oil-rich and a water-rich stream. Two co-current swirl separators, one for each stream, perform further purification of the product streams from the gravity separator to produce the final products. Models are developed for each of the separators in the system. These are based on the average velocity of the droplets estimated by the buoyancy forces and the drag forces approximated by Stokes' law. The models require a correlation between the viscosity and the oil volume fraction of the emulsion. The average droplet size in the swirl separators is assumed to be dependent on the maximum tangential velocity present in the separator and a correlation between these values is required.

The model of the swirl separator for oil-in-water emulsions is validated by comparison to experimental data provided by van Campen [18]. The experiments are run at different flow rates, flow splits, inlet oil cuts and with different swirl elements. The model generally shows good agreement with the experimental data. It does, however, deviate from the experimental values when the inlet oil cut is close to the point of phase inversion (i.e., large values of α_{in}). The model also shows reduced accuracy at low oil cuts in the inlet stream (i.e., $\alpha \approx 0.1$), but the deviation in this region is less consistent and depends on the flow rate and swirl element.

The separation system is optimized for the oil volume fraction in the oil-rich product, with the water-rich product constrained to contain

less than 3% oil. The optimization variables are the flow splits of each separator. The optimal flow splits are in general found to be close to the oil cut in the inlet of the respective separators. However, the estimated optima show that other factors affect the ideal flow splits. The optimal flow splits are highly dependent on the ideal inlet flow rate to the swirl separators, i.e., the flow rate where the enhancing effect of the increased centrifugal acceleration balances out the reducing effect of the droplet break-up and the reduced residence time.

6.1 Further Work

The models for the gravity separator and the swirl separator for continuous oil phase are not validated with experimental data. This should be done to determine the accuracy of these models. Possible adjustments/improvements to the models should be assessed on the basis of the experimental results.

More experimental work on the swirl separator for continuous water phase can improve this model. There are some data available for varying flow rates, but more measurements at a wider range of flow rates are needed in order to identify the local maxima of the separation efficiency. The accuracy of the simulated maxima is essential for the optimizer and should thus be examined thoroughly. Possible experimental work might also help us understand the inaccuracy of the model at low inlet oil cuts (i.e., $\alpha_{in} < 0.2$) if the experiments are carried out at these conditions. The accuracy of the model at low oil cuts is important for the studied optimization procedure.

A control structure of the separation system should be proposed and evaluated on the basis of the model. The control variables should be chosen in such a way that the system is *self-optimizing*. That is, the loss (compared to the true optimum) is *acceptable* with constant set point values (without the need to reoptimize when disturbances occur) [15].

Bibliography

[1] Arirachakaran, S., Oglesby, K., Malinowsky, M., Shoham, O., Brill, J., 1989. An analysis of oil/water flow phenomena in horizontal pipes. In: SPE Production Operations Symposium, 13-14 March, Oklahoma City, Oklahoma. Society of Petroleum Engineers, SPE. URL https://www.onepetro.org/conference-paper/SPE-18836-MS

[2] Balakrishna, S., Biegler, L. T., 1992. Targeting strategies for the synthesis and energy integration of nonisothermal reactor networks. Industrial & Engineering Chemistry Research 31 (9), 2152–2164. URL http://dx.doi.org/10.1021/ie00009a013

[3] Constantinides, A., Mostoufi, N., 1999. Numerical Methods for Chemical Engineers with MATLAB Applications. Prentice Hall PTR, Prentice-HAll Inc., Upper Saddle River, New Jersey.

[4] Davies, J., 1985. Drop sizes of emulsions related to turbulent energy dissipation rates. Chemical Engineering Science 40 (5), 839 – 842. URL http://www.sciencedirect.com/science/article/pii/0009250985850363

[5] Dirkzwager, M., December 1996. A New Axial Cyclone Design for Fluid-Fluid Separation. Ph.D. thesis, Delft University of Technology.

[6] Hinze, J. O., 1955. Fundamentals of the hydrodynamic mechanism of splitting in dispersion processes. AIChE Journal 1 (3), 289–295. URL http://dx.doi.org/10.1002/aic.690010303

[7] Ishii, M., Zuber, N., 1979. Drag coefficient and relative velocity in

bubbly, droplet or particulate flows. AIChE Journal 25 (5), 843–855.
URL http://dx.doi.org/10.1002/aic.690250513

[8] MathWorks, Inc., 2015. Documentation: fmincon. Accessed: 2015-05-29.
URL http://se.mathworks.com/help/optim/ug/fmincon.html

[9] McClimans, O., Fantoft, R., 2006. Status and new developments in subsea processing. In: Offshore Technology Conference, 1-4 May, Houston, Texas, USA.
URL https://www.onepetro.org/conference-paper/OTC-17984-MS

[10] Moreno-Trejo, J., Markeset, T., 2012. Identifying challenges in the development of subsea petroleum production systems. In: Frick, J., Laugen, B. (Eds.), Advances in Production Management Systems. Value Networks: Innovation, Technologies, and Management. Vol. 384 of IFIP Advances in Information and Communication Technology. Springer Berlin Heidelberg, pp. 287–295.
URL http://dx.doi.org/10.1007/978-3-642-33980-6_33

[11] Mørk, P. C., 1999. Overflate og kolloidkjemi : grunnleggende prinsipper og teorier. Norwegian University of Science and Technology, Department of Chemical Engineering, Trondheim, Norway.

[12] Najafi, A., Mousavian, S., Amini, K., 2011. Numerical investigations on swirl intensity decay rate for turbulent swirling flow in a fixed pipe. International Journal of Mechanical Sciences 53 (10), 801 – 811.
URL http://www.sciencedirect.com/science/article/pii/S0020740311001305

[13] Petroleum Safety Authority Norway, 2001. Regulations relating to conducting petroleum activities. Accessed: 2015-05-27.
URL http://www.ptil.no/aktivitetsforskriften/aktivitetsforskriften-e2007-n-article3868-379.html

[14] Sherman, P., 1962. The viscosity of emulsions. Rheologica Acta 2 (1), 74–82.
URL http://dx.doi.org/10.1007/BF01972558

[15] Skogestad, S., 2000. Plantwide control: the search for the self-optimizing control structure. Journal of Process Control 10 (5), 487 – 507.
URL http://www.sciencedirect.com/science/article/pii/S0959152400000238

[16] Slot, J. J., October 2013. Development of a Centrifugal In-Line Separator for Oil-Water Flows. Ph.D. thesis, University of Twente.

[17] Statoil ASA, 2015. Subsea processing on Tordis. Accessed: 2015-06-03.
URL http://www.statoil.com/en/TechnologyInnovation/FieldDevelopment/AboutSubsea/SubseaProcessingOnTordisIOR/Pages/default.aspx

[18] van Campen, L., January 2014. Bulk Dynamics of Droplets in Liquid-Liquid Axial Cyclones. Ph.D. thesis, Delft University of Technology.

[19] van Campen, L., Mudde, P. R., dr.ir. J.J. Slot, prof.dr.ir. H.W.M. Hoeijmakers, 2012. A numerical and experimental survey of a liquid-liquid axial cyclone. International journal of chemical reactor engineering 10 (1).
URL http://doc.utwente.nl/83139/

[20] Woelflin, W., 1942. The viscosity of crude-oil emulsions. In: Drilling and Production Practice, 1 January, New York, New York. American Petroleum Institute, API.
URL `https://www.onepetro.org/conference-paper/API-42-148`

A Derivation of the Oil Cut Equation

The average oil volume fraction on the inside of a droplet moving through the separator is derived by assuming that no droplet paths cross each other. Considering a droplet entering the separator at $r = r_{in}$ and exiting at R_i. At an arbitrary point in time it is located at $r = r_1$ (see Figure A.1). The flux of oil droplets going through the circular cross section defined by R_i will than be equal to the flux of oil droplets going through the cross section defined by r_1. This is stated mathematically in equation A.1 and rewritten to equation A.2 by inserting symbols.

$$\begin{aligned}&(\text{Oil flux between } r_{in} \text{ and } R_i) \ + (\text{Oil flux inside } R_i) \ = \\ &(\text{Oil flux between } r_1 \text{ and } R_i) \ + (\text{Oil flux inside } R_i)\end{aligned} \tag{A.1}$$

$$\begin{aligned}&\alpha_{in} \cdot \frac{r_{in}^2 - R_i^2}{R^2 - R_i^2} \cdot q_{HPO} + \alpha_{in} \cdot q_{LPO} = \\ &\alpha_1 \cdot \frac{r_1^2 - R_i^2}{R^2 - R_i^2} \cdot q_{HPO} + \alpha_1 \cdot q_{LPO}\end{aligned} \tag{A.2}$$

Here, α_{in} and α_1 are the average oil volume fractions inside the droplet at the inlet and at position 1, respectively. $q_{LPO} = FS \cdot q_{in}$ and $q_{HPO} = (1 - FS) \cdot q_{in}$ are the respective volumetric flow rates of the LPO and HPO. Equation A.2 can be simplified to equation A.3 by dividing by q_{in} and solving for α_1.

$$\alpha_1 = \alpha_{in} \frac{FS(R^2 - R_i^2) + (1 - FS)(r_{in}^2 - R_i^2)}{(1 - FS)(r_1^2 - R_i^2) + FS(R^2 - R_i^2)} \tag{A.3}$$

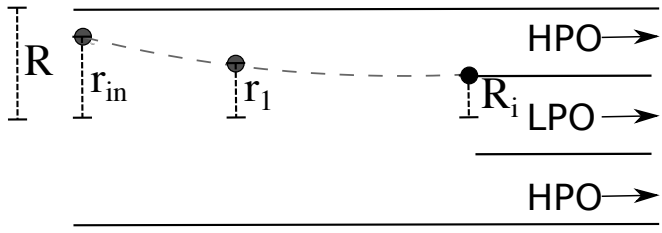

Figure A.1: Droplet path trough the separator. The droplet enters at the radial position r_{in} and exits at R_i. The radial position of the droplet at an arbitrary point in time is r_1.

B Integration Method

In order to do optimization, each evaluation of the separator function needs to be fast. Therefore, a constant time step, explicit, second order Runge-Kutta integrator has been developed for calculating the droplet paths. The actual MATLAB function can be found in Appendix C.5.1.

To validate the integrator, it is compared to the embedded MATLAB functions ode23 and ode45 in Figure B.1. The path of oil droplet in the continuous water separator is simulated for a droplet entering the separator at $t = 0\,\mathrm{s}$ and $r = 0.05\,\mathrm{m}$. The large swirl element is used with a flow rate of 10 m^3/h and an inlet oil volume fraction of 0.3. The flow split is also set to 0.3. The droplet paths follow each other quite close through the separator. With the level of uncertainty already present in a relatively crude model as this, the integrator performance is more than sufficient. It can be seen from Table B.1 that the used integrator uses the lowest amount of integration step of the three and the the radial position of the droplet at the outlet deviates with less than 0.4%.

Table B.1: Comparison of the used integrator (RK2) to the MATLAB integrators ode23 and ode45. The radial position of the droplet at the exit, $r(t = \tau)$, deviates with less than 0.4%.

Integrator	Steps	$r(t = \tau)$ [mm]	Constant Time Step
RK2	10	28.4	Yes
ode23	11	28.3	No
ode45	40	28.3	No

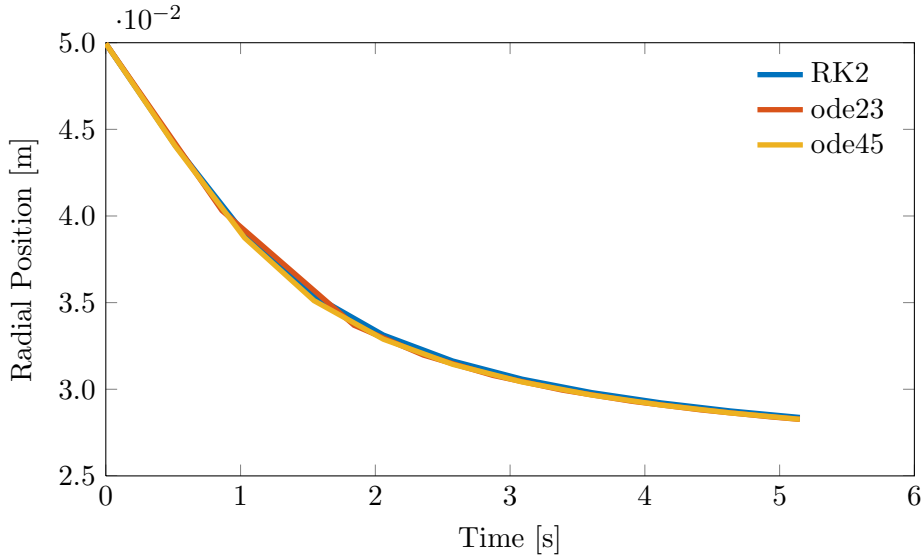

Figure B.1: Comparison of droplet path through separator with three different integrators. The constant time step, second order Runge-Kutta integrator (RK2) is used in the model. The integrator is compared to the embedded MATLAB integrators ode23 and ode45.

C MATLAB Code

This appendix contains the MATLAB code used in context of the thesis. The scripts used to estimate the outlet oil cuts of the respective separators are listed in:

- Appendix C.1: Oil-in-water swirl separator.
- Appendix C.2: Water-in-oil swirl separator.
- Appendix C.3: Gravity separator.

The optimization procedure is presented in Appendix C.4 and the solvers are listed in Appendix C.5.

C.1 Oil-in-Water Swirl Separator

This section contains the MATLAB scripts used to estimate the separation of the swirl separator for oil-in-water emulsions. The main function (Appendix C.1.1) calls the function containing the differential equation for the droplets (Appendix C.1.2) and the function that estimates the composition in the outlet streams (Appendix C.1.3). Two solvers are also required to solve the necessary equations, these are presented in Appendix C.5.

C.1.1 Main function

The function *swirl_func3* estimates the condition of the outlet streams of the oil-in-water swirl separator given a set of inlet conditions.

```
1 function [Vo_LPO,Vo_HPO,Edil,Edis,qen]=...
```

```
2  swirl_func3(Vo_in,qin,FS,element)
3  %% Input:
4  % Inlet oil cut (Vo_in [-])
5  % Inlet flow rate (qin [m^3/s])
6  % Flow split (FS [-])
7  % Swirl element (element: 'w', 's' or 'l')
8  %% Output:
9  % LPO oil cut (Vo_LPO [-])
10 % HPO oil cut (Vo_HPO [-])
11 % Dilute efficiency (Edil [-])
12 % Dispersed efficiency (Edis [-])
13 %% Code:
14
15 Lsw=1.7;
16 Ro=0.05;
17 Ri=0.025;
18
19 qi=FS*qin; %Light phase out flow
20 qo=qin-qi;    %Heavy phase out flow
21 ta=pi*(Ro^2-Ri^2)*Lsw/qo;
22
23 % Check for total separation
24 rin=0.999*Ro;
25 x0=[rin];
26 M=zeros(length(x0));
27 M(1,1)=1;
28 options = odeset;
29 in=[qin,Ro,Ri,Vo_in,ta,rin,FS];
30 h=ta/10;
31 [T,X]=RK2(@swirl_sep2,[0 ta],x0,h,in,element);
32 %[T,X]=ode23(@swirl_sep2,[0 ta],x0,options,in,element);
33
34 %Finding r(t0) that gives r(ta)=Ri
35 if X(end,1)>Ri && X(end,1)<Ro %
36     TotSep=0; %Not total separation
```

```
37      rin_0=0.99*Ro;%Ri+0.5*(Ro-Ri);%[0.038,0.039];%
38      rho=1;
39      tol=10^-10*Ri;
40      [T,X]=shooting...
41      (@swirl_sep2,[0,ta],h,Ri,rin_0,rho,tol,in,element);
42      rin=X(1,1);
43  else
44      TotSep=1;
45      rin=Ro;
46  end
47  p2=[Lsw;Ro;Ri];
48  [Vo_LPO,Vo_HPO,qen]=DeOiler(qin,Vo_in,FS,rin,p2);
49
50  Edil=Vo_LPO*qi/(Vo_in*qin);
51  Edis=1-((1-Vo_LPO)*qi+Vo_HPO*qo)/qin;
```

C.1.2 Governing Equation

The function *swirl_sep2* contains the majority of the model equations for the oil-in-water swirl separator. The function returns the radial velocity of a droplet in the separator given a set of conditions.

```
1  function [DXDT]=swirl_sep2(t,x,in,element)
2  qin=in(1); Ro=in(2); Ri=in(3);
3  Vo_in=in(4); ta=in(5); rin=in(6); FS=in(7);
4
5  rhoo=881; rhow=1064; %kg/m^3
6  muw=1*10^-3; muo=16.7*10^-3;%Pa*s
7
8  r=x(1);
9
10 Rc=0.25*Ro;
```

```
va=qin/(pi*Ro^2);
if element=='w' %weak
    k=3.5;
elseif element=='s' %strong
    k=5;
elseif element=='l' %large
    k=7;
end

vt=k*va;

%Experimental correlation between rd and vt
if vt>4.45%28
    rd=(-8*vt+160)/2*10^-6;
else
    rd=(-107*vt+600)/2*10^-6;
end

va=qin*(1-FS)/(pi*(Ro^2-Ri^2));
Vo_c=Vo_in*(FS*(Ro^2-Ri^2)*(Ro^2-r^2)...
    +(rin^2-Ri^2)*(Ro^2-r^2)*(1-FS))...
    /((r^2-Ri^2)*(Ro^2-r^2)*(1-FS)+FS*(Ro^2-Ri^2)*(Ro^2-r^2));

mum=(0.47*Vo_c^3-0.4*Vo_c^2+0.11*Vo_c+0.001);

vr=((2/9*(rhoo-rhow)*rd^2/(mum)...
    *(vt*exp(-0.04*va*t/(2*Ro)))^2/r)...
    *heaviside(r-Rc)... %r>Rc
    +(2/9*(rhoo-rhow)*rd^2/mum...
    *r*(vt*exp(-0.04*va*t/(2*Ro))/Rc)^2)...
    *heaviside(Rc-r))... %r<Rc
    *heaviside(r-0.9*Ri); %To make sure r>0

DXDT=[vr];
end
```

C.1.3 Outlet Oil Cuts

The function *DeOiler* estimates the outlet composition given the greatest inlet radial position of all the droplets that exit in the LPO.

```
function [Vo_LPO,Vo_HPO,qen]=DeOiler(qin,Vo_in,FS,rin,p2)
Ro=p2(2);Ri=p2(3);

qi=FS*qin; qo=qin-qi;

Vo_LPO=Vo_in*(FS*(Ro^2-Ri^2)+(rin^2-Ri^2)*(1-FS))...
    /(FS*(Ro^2-Ri^2));
Vo_HPO=(Vo_in*qin-Vo_LPO*qi)/qo;
u_HPO=qo/(pi*(Ro^2-Ri^2));u_LPO=qi/(pi*Ri^2);

du=(u_LPO-u_HPO);

k=2*10^-4;
qen=k*du;
if du>=0
    Vo_LPO=(Vo_LPO*(qi-qen)+Vo_HPO*qen)/qi;
else
    Vo_HPO=(Vo_HPO*(qo+qen)-Vo_LPO*qen)/qo;
    Vo_LPO=(Vo_in*qin-Vo_HPO*qo)/qi;
end

if Vo_LPO>1
    Vo_LPO=1;
elseif Vo_LPO<Vo_in
    Vo_LPO=Vo_in;
end

Vo_HPO=(Vo_in*qin-Vo_LPO*qi)/qo;
```

```
29 end
```

C.2 Oil-in-Water Swirl Separator

This section contains the MATLAB scripts used to estimate the degree of separation of the swirl separator for water-in-oil emulsions. The main function (Appendix C.2.1) calls the function containing the differential equation for the droplets (Appendix C.2.2) and the function that estimates the composition in the outlet streams (Appendix C.2.3). It also calls the solvers listed in Appendix C.5.

C.2.1 Main Function

The function *swirl_func3_o* estimates the condition of the outlet streams of the water-in-oil swirl separator given a set of inlet conditions.

```
1  function [Vw_LPO,Vw_HPO,Edil,Edis,qen]=...
2      swirl_func3_o(Vo_in,qin,FS,element)
3  Lsw=1.7;
4  Ro=0.05;
5  Ri=0.043;
6
7  qi=FS*qin;       %Light phase out flow
8  qo=qin-qi;       %Heavy phase out flow
9  ta=pi*Ri^2*Lsw/qi;
10
11 %Finding r(t0) that gives r(ta)=Ri
12 h=ta/10;
13 rin_0=0.8*Ri;
14 in=[qin,Ro,Ri,Vo_in,ta,rin_0,FS];
```

```
15 rho=1;
16 tol=10^-10*Ri;
17 [T,X]=shooting...
18     (@swirl_sep2_o,[0,ta],h,Ri,rin_0,rho,tol,in,element);
19
20 rin=X(1,1);
21
22
23 [Vo_LPO,Vo_HPO,qen]=DeWaterer(qin,Vo_in,FS,rin,[Lsw;Ro;Ri]);
24 Vw_LPO=1-Vo_LPO; Vw_HPO=1-Vo_HPO;
25
26 Edil=Vw_HPO*qo/((1-Vo_in)*qin);
27 Edis=1-((1-Vo_LPO)*qi+Vo_HPO*qo)/qin;
```

C.2.2 Governing Equation

The function *swirl_sep2_o* contains the majority of the model equation for the water-in-oil swirl separator. The function returns the radial velocity of a droplet in the separator given a set of conditions.

```
1  function [vr]=swirl_sep2_o(t,x,in,element)
2  qin=in(1);
3  Ro=in(2);
4  Ri=in(3);
5  Vo_in=in(4);
6  ta=in(5);
7  rin=in(6);
8  FS=in(7);
9
10 Vw_in=(1-Vo_in);
11
12 rhoo=881; %kg/m^3
```

```
13 rhow=1064;
14 muw=1*10^-3; %Pa*s
15 muo=10*10^-3;
16
17 r=x(1);
18
19 Rc=0.25*Ro;
20 va=qin/(pi*Ro^2);
21 if element=='w' %weak
22     k=3.5;
23 elseif element=='s' %strong
24     k=5;
25 elseif element=='l' %large
26     k=7;
27 end
28
29 vt0=k*va;
30
31 %Experimental correlation between rd and vt
32 if vt0>4.45%28
33     rd=(-8*vt0+160)/2*10^-6;
34 else
35     rd=(-107*vt0+600)/2*10^-6;
36 end
37
38
39 Vw=Vw_in*(((1-FS)*Ri^2+FS*(Ri^2-rin^2))...
40     /((1-FS)*Ri^2+FS*(Ri^2-r^2)));
41
42 mum=(0.203*Vw^3+0.237*Vw^2-0.014*Vw+0.0088);
43
44 f2=(vt0*exp(-0.04*va*t/(2*Ro)))^2/r;
45 f1=(vt0*exp(-0.04*va*t/(2*Ro))/Rc)^2*r;
46 f=f2-f1; beta=10;
47 ac=f2-0.5*((f^2+beta^2)^.5+f);
```

```
% vt=sqrt(ac*r);
vr=2/9*(rhow-rhoo)*rd^2/mum*ac;
end
```

C.2.3 Outlet Oil Cuts

The function *DeWaterer* estimates the outlet composition given the lowest inlet radial position of all the droplets that exit in the HPO.

```
function [Vo_LPO,Vo_HPO,qen]=DeWaterer(qin,Vo_in,FS,rin,p3)

Ro=p3(2);Ri=p3(3);

qi=FS*qin;       %Light phase out flow
qo=qin-qi;       %Heavy phase out flow


Vw_HPO=...
    (1-Vo_in)*(((1-FS)*Ri^2+FS*(Ri^2-rin^2))/((1-FS)*Ri^2));
Vw_LPO=((1-Vo_in)*qin-Vw_HPO*qo)/qi;

u_LPO=qi/(pi*Ri^2);
u_HPO=qo/(pi*(Ro^2-Ri^2));
du=u_LPO-u_HPO;
k=2*10^-4;
qen=k*du;

%Re-Entrainment
if du>0
    Vw_LPO=(Vw_LPO*(qi-qen)+Vw_HPO*qen)/qi;
    Vw_HPO=((1-Vo_in)*qin-Vw_LPO*qi)/qo;
else
    Vw_HPO=(Vw_HPO*(qi+qen)-Vw_LPO*qen)/qi;
```

```
25 end
26
27 % Restrict volume fraction to range 0->1
28 if Vw_HPO>1
29     Vw_HPO=1;
30 elseif Vw_HPO<(1-Vo_in)
31     Vw_HPO=(1-Vo_in);
32 end
33
34 Vw_LPO=((1-Vo_in)*qin-Vw_HPO*qo)/qi;
35
36 Vo_LPO=1-Vw_LPO;
37 Vo_HPO=1-Vw_HPO;
38 end
```

C.3 Gravity Separator

The function *gravity_sep2* returns the oil cut in the top and bottom outlet of the gravity separator provided the inlet conditions and flow split of the separator.

```
1  function [Vo_t,Vo_b]=gavity_sep2(FS,qin,Vo_in)
2  Lsep=7;
3  R=1.7;
4  Hw=0.75*2*R;
5  g=-9.81;
6
7  qt=FS*qin;qb=qin-qt;
8
9  rhoo=881;rhow=1064;%kg/m^3
10
11 mum=(0.6*Vo_in^3-0.506*Vo_in^2+0.137*Vo_in+0.001); %Pa*s
```

```
12 rd=60*10^-6; %m^3
13
14 AHw=R^2/2*((2*acos((R-Hw)/R))-sin(2*acos((R-Hw)/R)));
15 vh=qb/AHw;
16 vv=2*g*(rhoo-rhow)*rd^2/(9*mum);
17
18 h=Lsep*vv/vh;
19
20 d=max(Hw-h,0);
21 Ad=R^2/2*((2*acos((R-d)/R))-sin(2*acos((R-d)/R)));
22
23 Vw_b=((AHw-Ad)/AHw+Ad/AHw*(1-Vo_in));
24 Vo_b=1-Vw_b;
25
26 Vo_t=(Vo_in-Vo_b*(1-FS))/FS;
27 if Vo_t>1
28     Vo_t=1;
29     Vo_b=(Vo_in-Vo_t*FS)/(1-FS);
30 end
31 end
```

C.4 Optimization

The separation system is optimized by running the optimization script (section C.4.1). The optimization script minimizes the cost function (section C.4.4) while satisfying the constraints given by the constraint function (section C.4.3). A function that finds an initial guess that satisfies the constraints is also included in the optimization procedure (section C.4.2).

C.4.1 Main Script

The main script minimizes the function *CostFunc2* under the constraints given by *constraints2* for a given set of inlet conditions. The cost function is minimized using the embedded MATLAB-function *fmincon* and the *interior point* algorithm.

```
1  qin=[20:0.25:26]/3600;
2  Vo_in=[0.4:0.0125:0.6];
3  Lsw=1.7;Ro=0.05;Ri=0.025;p2=[Lsw;Ro;Ri];
4  Lsw_DW=1.7;Ro_DW=0.05;Ri_DW=0.043;p3=[Lsw_DW;Ro_DW;Ri_DW];
5
6  element='1';
7
8  x=zeros(length(qin),length(Vo_in),21);
9  comp=zeros(length(qin),length(Vo_in),6);
10 exitflag=zeros(length(qin),length(Vo_in));
11 Cost=zeros(length(qin),length(Vo_in));
12 options =...
13     optimset('Algorithm','interior-point','Display','off');
14 A=[];b=[];Aeq=[];beq=[];
15
16
17 %Optimization
18 for j=1:length(Vo_in)
19     for i=1:length(qin)
20         p=[qin(i);Vo_in(j)];
21         % Bounds for inputs
22         %The bounadries on the FSs are just to help the solver
23         %and should not be active!!
24         lb=[0.1;0.5;0;0.1;p2(3);zeros(16,1)];
25         ub=zeros(21,1);
26         ub(1:5,1)=[0.9;0.95;p3(3);0.6;p2(2)];
```

```
27          for k =6:length(ub)
28              a=factor(k);
29              if a(1)==2; %flow
30                  ub(k,1)=qin(i);
31              else %volume fraction
32                  ub(k,1)=1;
33              end
34          end
35          %Initial guess
36          if j==1 && i==1
37              %  FS_g,FS_DW,rin_DW,FS_DO,rin_DO
38              x01=[Vo_in(i);0.8;0.4*Ri_DW;0.3;0.65*Ro];
39              x0=InitialGuess(x01,p,p2,p3);
40          elseif i==1 && j≠1
41              x0=x02;
42          end
43          [x(i,j,:),¬,exitflag(i,j),output(i,j)] = fmincon(...
44              @(x)CostFunc2(x,p,p2,p3),x0,A,b,Aeq,beq,lb,ub,...
45              @(x)constraints2(x,p,p2,p3,element),options);
46          [Cost(i,j)]=CostFunc2(x(i,j,:),p,p2,p3);
47          if exitflag(i,j)==1 ||exitflag(i,j)==2
48              x0=squeeze(x(i,j,:));
49          end
50          if j==1
51              x02=x0;
52          end
53      end
54  end
```

C.4.2 Initial Guess Function

The function *InitialGuess* finds 18 values of the state vector that are consistent with the first five. If the initial guess is inconsistent (i.e., the

constraint are not satisfied), *fmincon* will shift the initial guess to satisfy the constraint function, which might give it undesirable values.

C.4.3 Constraint Function

The function *constraints2* include all the equations in the model of the separation system and additional inequality constraints set on the purity of the streams. It calls the functions related to the three separators.

```
function [c,ceq]=constraints2(x,p,p2,p3,element)
FS_g=x(1);FS_DW=x(2);rin_DW=x(3);FS=x(4);rin=x(5);
qin=p(1);Vo_in=p(2);
Lsw=p2(1);Ro=p2(2);Ri=p2(3);
Lsw_DW=p3(1);Ro_DW=p3(2);Ri_DW=p3(3);

%Gravity
[Vo_t,Vo_b]=gavity_sep2(FS_g,qin,Vo_in);
qb=(1-FS_g)*qin;
qt=qin-qb;
%DeWaterer
qi_DW=FS_DW*qt; %Light phase out flow
qo_DW=qt-qi_DW;     %Heavy phase out flow
ta_DW=pi*Ri_DW^2*Lsw_DW/qi_DW;

options = odeset;
in_DW=[qt,Ro_DW,Ri_DW,Vo_t,ta_DW,rin_DW,FS_DW];
h_DW=ta_DW/10;
[T,X_DW]=...
    RK2(@swirl_sep2_o,[0 ta_DW],rin_DW,h_DW,in_DW,element);
options = odeset('AbsTol',10^-6);
```

```
%[T,X_DW]=
%ode45(@swirl_sep2_o,[0 ta_DW],rin_DW,options,in_DW,element);

[Vo_LPO_DW,Vo_HPO_DW]=DeWaterer(qt,Vo_t,FS_DW,rin_DW,p3);


rout_DW=X_DW(end,1);

%DeOiler
q3=qb+qo_DW;
Vo_3=(Vo_b*qb+Vo_HPO_DW*qo_DW)/q3;
qi=FS*q3; %Light phase out flow
qo=q3-qi;    %Heavy phase out flow
ta=pi*(Ro^2-Ri^2)*Lsw/qo;

options = odeset;
in=[q3,Ro,Ri,Vo_3,ta,rin,FS];
h=ta/10;
[T,X]=RK2(@swirl_sep2,[0 ta],rin,h,in,element);
%[T,X]=ode45(@swirl_sep2,[0 ta],rin,options,in,element);
rout=X(end,1);
[Vo_LPO_DO,Vo_HPO_DO]=DeOiler(q3,Vo_3,FS,rin,p2);

%Oil Product
qoil=qi_DW+qi;
Vo_oil=(Vo_LPO_DW*qi_DW+Vo_LPO_DO*qi)/qoil;

%constraints

%In case of fixed flow splits:
FSzero=[FS_g-0.33;FS_DW-0.91;FS-0.15];

ExplEq=[qt;Vo_t;qb;Vo_b;qi_DW;Vo_LPO_DW;...
    qo_DW;Vo_HPO_DW;q3;Vo_3;...
    qi;Vo_LPO_DO; qo; Vo_HPO_DO; qoil; Vo_oil]-x(6:21);
```

```
57 ceq=[(Ri_DW-rout_DW)/Ri_DW;(rout-Ri)/Ri;ExplEq];
58 c=[0.7-Vo_t;Vo_3-0.6;x(19)-0.03];%
59 end
```

C.4.4 Cost Function

The function *CostFunc2* is minimized by the main script.

```
1 function [c]=CostFunc2(x,p,p2,p3)
2 %x(21): Oil volume fraction in LPO
3 c=(1-x(21))*10;
4 end
```

C.5 Solvers

Two solvers are coded in order to solve the necessary equation in the models. The second order Runge-Kutta function is listed in section C.5.1, while the function used for the *shooting method* is listed in section C.5.2.

C.5.1 Runge-Kutta

The function *RK2* is a second order explicit Runge-Kutta solver, which is called by *swirl_func3* and *swirl_func3_o* to solve the differential equations for the droplets.

```
1 function [t,y]=RK2(ODEfile,tspan,yi,h,varargin)
2 %2nd order explicit Runge-Kutta
3 t=tspan(1):h:tspan(2);
4 if t(end)~=tspan(2)
```

```
5       t(end+1)=tspan(2);
6   end
7   d=diff(t);
8   yi=(yi(:).')';
9
10  y(:,1)=yi;
11  for i=1:length(t)-1
12      k1=d(i)*feval(ODEfile,t(i),y(:,i),varargin{:});
13      k2=d(i)*feval(ODEfile,t(i+1),y(:,i)+k1,varargin{:});
14      y(:,i+1)=y(:,i)+(k1+k2)/2;
15  end
16  y=y';
17  t=t';
18  end
```

C.5.2 Shooting Method

The function *shooting* is a numerical solver, which uses the Newton-Raphson method to solve boundary call problems. It is called by *swirl_func3* and *swirl_func3_o* to solve boundary value problem for the differential equations for the droplets.

```
1   function [t,y]=shooting...
2       (ODEfile,tspan,h,yf,gamma0,rho,tol,varargin)
3
4   gammanew=gamma0;
5   iter=0;
6   maxiter=100;
7   fnk=10*yf;
8   while max(abs(yf-fnk))>tol & iter<maxiter
9       iter=iter+1;
10      gamma1=gammanew;
```

```
11      varargin{1}(6)=gamma1; %Specific for swirl_sep2 in(6)=rin
12
13      [t,y]=RK2(ODEfile,tspan,gamma1,h,varargin{:});
14      fnk=y(end,1);
15          if gamma1≠0
16              dgamma=-gamma1/100;
17          else
18              dgamma=-0.01;
19          end
20      a=gamma1+dgamma;
21      varargin{1}(6)=a; %Specific for swirl_sep2 in(6)=rin
22      [ta,ya]=RK2(ODEfile,tspan,a,h,varargin{:});
23      fnka=ya(end,1);
24      jacob=(fnka-fnk)/dgamma;
25      a=gamma1-dgamma;
26      if jacob==0;
27          gammanew=gamma1+max([abs(dgamma),1.1*tol]);
28      else
29          gammanew=gamma1-rho*inv(jacob)*(fnk-yf);
30      end
31  end
32
33  if iter≥maxiter
34      disp(['Maximum iterations reached. (rout-Ri)/Ri= ',...
35          num2str((fnk-yf)/yf)])
36      disp(ODEfile)
37  end
38  end
```

D Investigation of the Re-Entrainment Rate

Re-entrainment is added to the model in order to compensate for over-simplifications made considering the flow patterns in the swirl separators. The rate of re-entrainment, $q_{re\text{-}en}$, is assumed to increase with increasing difference in the axial velocity of the LPO and the HPO, Δv. Two alternatives for the correlation between $q_{re\text{-}en}$ and Δv is investigated in this appendix. We consider Case A (equation D.1), which is a linear relationship and Case B (equation D.2), which is a quadratic relationship.

$$q_{re\text{-}en,A} = k_A \Delta v \tag{D.1}$$

$$q_{re\text{-}en,B} = k_B \Delta v \left|\Delta v\right| \tag{D.2}$$

The proportionality constants k_A and k_B were adjusted to give an optimal fit to experimental data from van Campen [18]. The experiment was run by increasing the oil content in the inlet while holding the flow rate constant. The flow spilt, FS, was adjusted to equal the inlet volume fraction of oil, α_{in}. Figure D.1a show the experimentally measured oil volume fractions in the LPO and HPO compared to the values predicted by the model with $k_A = 2 \cdot 10^{-4}\ m^2$ (Case A). Figure D.1b shows the same experimental data, but with the use of equation D.2 and $k_B = 5 \cdot 10^{-4}$ ms (Case B). For both cases, the model show good agreement with the experimental data. The model predictions *without* re-entrainment (i.e., $k = 0$) are presented in Figure D.2 and show significantly greater mismatch

than either of the cases with re-entrainment.

To determine which of Case A and B that better predicts the experimental data, another comparison is studied. The experiment has been conducted by van Campen [18] by changing the flow split gradually from 0.2 to 0.6 with constant inlet conditions. This allows us to see the effect of the flow split, and thus Δv, on the separation efficiency. Case A is compared to the experimental results in Figure D.3, while Case B is compared to the same data in Figure D.4. Case A shows good agreement with the experimentally obtained data with the same linear increase in η_{dil} (eq. 2.10) and linear decrease in η_{dis} (eq. 2.11) when the flow split increases. Case B does, on the other hand, show worse agreement with the experimental data. The model deviates more from the experimental data at high flow splits. This is a result of the quadratic nature of equation D.2. On this basis, Case A (equation D.1) is used in the final model.

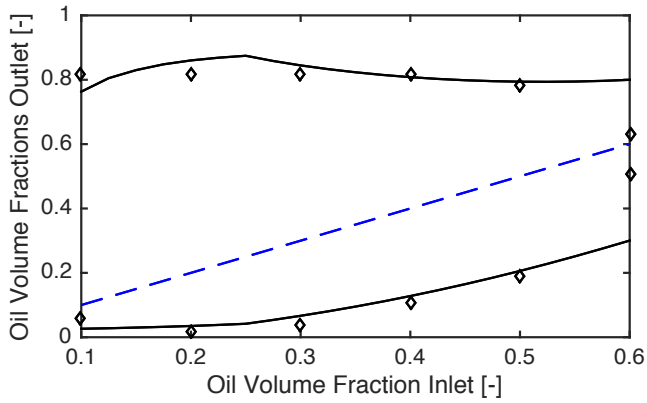

(a) Case A. $k_A = 2 \cdot 10^{-4}\ m^2$ was found to give the desired agreement with experimental data.

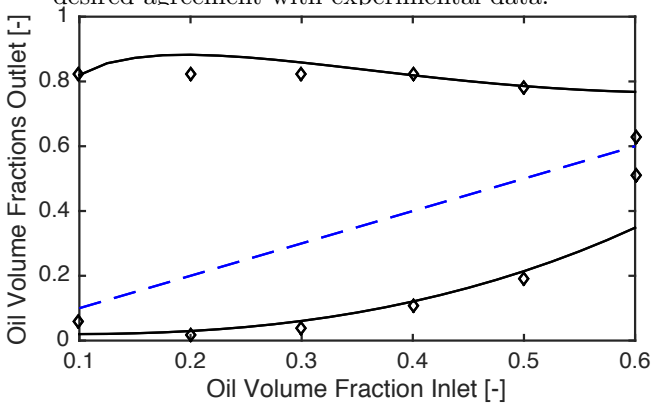

(b) Case B. $k_B = 5 \cdot 10^{-4}\ ms$ was found to give the desired agreement with experimental data.

Figure D.1: Model (solid line) and experimental values (diamonds) of α_{LPO} (above dashed line) and α_{HPO} (below dashed line) versus α_{in}. The large swirl element is used and the inlet flow rate is 10 m^3/h. The flow split is equal to the inlet oil volume fraction, $FS = \alpha_{in}$.

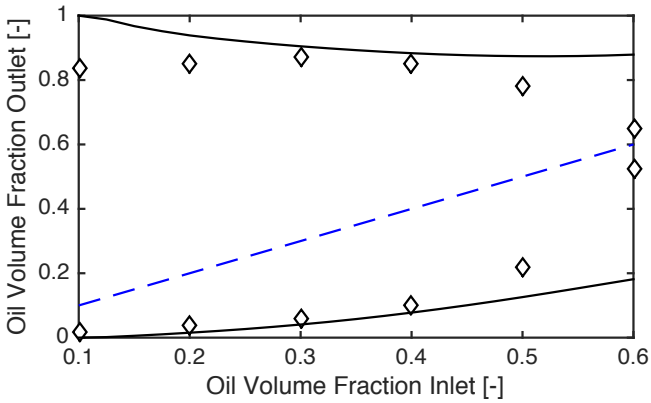

Figure D.2: Without re-entrainment. Model (solid line) and experimental values (diamonds) of α_{LPO} (above dashed line) and α_{HPO} (below dashed line) versus α_{in}. The large swirl element is used and the inlet flow rate is 10 m^3/h. The flow split is equal to the inlet oil volume fraction, $FS = \alpha_{in}$.

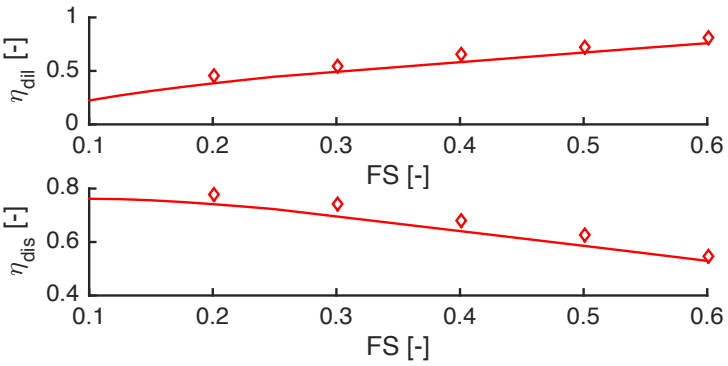

Figure D.3: Case A. Model (solid line) and experimental values (diamonds) of dispersed (upper) and dilute (lower) efficiency versus flow split. The strong swirl element is used and the inlet flow rate is 56.5 m^3/h and the inlet oil volume fraction is 0.25.The efficiencies are defined in equation 2.10 & 2.11.

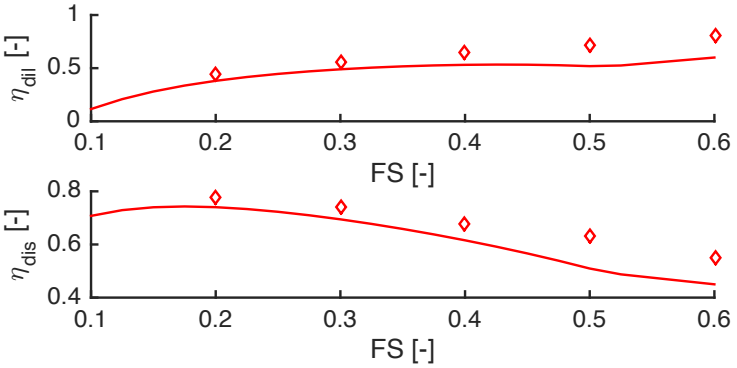

Figure D.4: Case B. Model (solid line) and experimental values (diamonds) of dispersed (upper) and dilute (lower) efficiency versus flow split. The strong swirl element is used and the inlet flow rate is 56.5 m^3/h and the inlet oil volume fraction is 0.25. The efficiencies are defined in equation 2.10 & 2.11.

E Model Error for Oil-in-Water Swirl Separator

The relative error of the model is dependent on what variable that is considered. The oil cuts in the outlet streams as a function of the inlet oil cuts, α_{in}, of the oil-in-water swirl separator are considered in Chapter 5.1.1. The simulated and experimental values are presented in Figure 5.2. In this case, the large swirl element is used and the separation is simulated for three different flow rates, q_{in}.

The simulations at $q_{in} = 30\,\mathrm{m^3\,h^{-1}}$ show the greatest deviation from the experimental data with the simulated oil cut in the LPO being more than twice of the experimental value at $\alpha_{in} = 0.1$. To demonstrate that the relative error of the model depends on which variable you consider, the dispersed efficiencies are presented in Table E.1. The error is here less than 9% at $\alpha_{in} = 0.1$, which should be considered an acceptable error for this type of model.

Table E.1: Experimental and simulated values of the dispersed efficiency at different oil volume fractions in the feed, α_{in}, for the oil-in-water swirl separator. Large swirl element, $q_{in} = 30\ m^3/h$ & $FS = \alpha_{in}$. The error of the model is given as: $\left(\eta_{dis}^{model}/\eta_{dis}^{experiment} - 1\right) \cdot 100\%$. The values of dispersed efficiency are displayed as a plot if Figure 5.3. Experimental values are provided by van Campen [18].

α_{in} [-]	$\eta_{dis}^{experiment}$ [-]	η_{dis}^{model} [-]	Error [%]
0.1	0.81	0.88	8.7
0.2	0.76	0.81	7.1
0.3	0.70	0.76	8.3
0.4	0.65	0.70	7.3
0.5	0.58	0.65	12
0.6	0.55	0.63	15

F Investigation of the Water-in-Oil Swirl Separator

There are no available experimental data for the water-in-oil swirl separator modeled in this thesis. The verification of the model is therefore challenging. However, experiments have been run by van Campen [18] for the separator originally designed for oil-in-water emulsions at oil cuts greater than 0.66 (i.e., with water-in-oil emulsions). The only difference between the physical dimensions of the two modeled swirl separators is that the radius of the pickup tube (R_i) is greater for the water-in-oil separator. Simulations are therefore executed for the water-in-oil separator with R_i =0.025 m, which is the size used in the experiment.

The re-entrainment rate (see Chapter 3.1.7) is estimated by assuming proportionality to the velocity difference of the LPO and HPO flow, Δv (eq. 3.15). The linearization is performed around $FS = (R_i/R)^2$ where $\Delta v = 0$ so the quality of the assumption will decrease for $FS \gg (R_i/R)^2$. The experiments considered in this appendix are performed for flow splits between 0.7 and 0.9 while $(R_i/R)^2 = 0.25$. The equation for the re-entrainment rate (eq. 3.15) must therefore be questioned. The simulations have as a consequence of this been executed with and without re-entrainment.

The experiment is performed with a constant flow rate of $10\,\mathrm{m^3\,h^{-1}}$ and the large swirl element. The flow split is kept equal to the oil cut in the feed. The dispersed efficiencies, $\eta_{dis}^{experiment}$, for three different oil cuts are listed in Table F.1 along the simulated values with, $\eta_{dis}^{re\text{-}en}$, and

Table F.1: The dispersed efficiency, η_{dis}, of a water-in-oil swirl separator for different oil cuts in the inlet, α_{in}. The radius of the pick-up tube is $R_i = 0.025\,\mathrm{m}$ (Note that this is not the same as the hypothetical separator used in the rest of this thesis). The flow rate is $q_{in} = 10\,\mathrm{m^3\,h^{-1}}$. $FS = \alpha_{in}$. Large swirl element. The simulations are performed with and without re-entrainment (eq. 3.15). The errors are given as the relative error to the experimental value.

α_{in} [-]	$\eta_{dis}^{experiment}$ [-]	$\eta_{dis}^{re\text{-}en}$ [-]	Error $\eta_{dis}^{re\text{-}en}$ [%]	η'_{dis} [-]	Error η'_{dis} [%]
0.73	0.63	0.74	17	0.80	27
0.79	0.80	0.77	-3.5	0.85	6.9
0.90	0.93	0.82	-12	0.96	2.9

without, η'_{dis}, re-entrainment. As expected, the model overestimates the separation efficiency close to the point of phase inversion. The same behavior is observed for the oil-in-water separator and is caused by the complex behavior of the emulsion at these conditions. The models show better accuracy when the oil cut in the feed is increased. The model with re-entrainment under predicts the separation efficiency while the model without re-entrainment over predicts the efficiency. This indicates that there is some degree of re-entrainment present is the separator, but that the used correlation overestimates the re-entrainment rate. This is expected as the re-entrainment expression (eq. 3.15) is linearized around $FS = (R_i/R)^2 = 0.25$. The statement is supported by the increased mismatch for FS=0.9 compared to FS=0.79.

Overall, the model seems to do reasonably accurate predictions, excluding the re-entrainment rate. The model for the water-in-oil separator consid-

ered in the rest of this thesis is not expected to have the same problems with predicting the re-entrainment rate as the radius of the pickup tube is increased to give $(R_i/R)^2 \approx 0.74$. The results presented in Table F.1 are therefore a good indication of the model being within the required accuracy. More experimental data are, however, required to give a sufficient verification of the model.

G Estimated Values of Optimal Conditions

The estimated conditions (i.e, flow rates & oil cuts) of the separation system (Chapter 3.5) for disturbances in the inlet oil cut and flow rate are listed in Table G.1 and G.2, respectively. The names of each stream are illustrated in the flow diagram in Figure G.1.

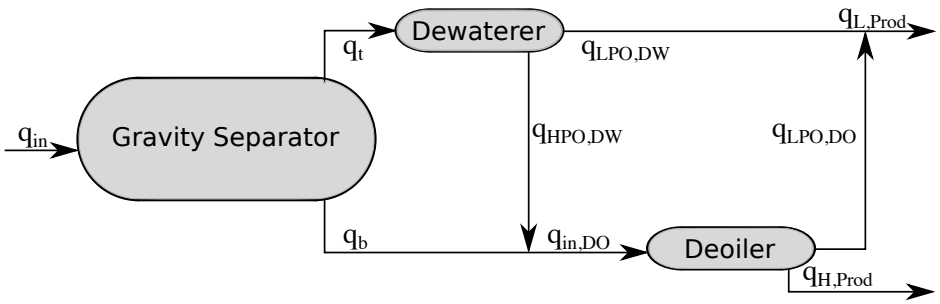

Figure G.1: Flow diagram for the separation system. The subscript of each stream corresponds to the values listed in Table G.1 and G.2.

Table G.1: Optimal operation for two different oil cuts in the inlet flow with q_{in}=20 $m^3\,h^{-1}$. The estimated flow splits (FS), oil cuts (α) and flow rates (q) for all the streams in the separation system are included.

Variable	α_{in}= 0.4	α_{in}= 0.5
FS_G [-]	0.33	0.40
α_t [-]	0.94	0.91
q_t [$m^3\,h^{-1}$]	6.7	8.0
α_b [-]	0.13	0.22
q_b [$m^3\,h^{-1}$]	13.3	12.0
FS_{DW} [-]	0.91	0.86
$\alpha_{LPO,DW}$ [-]	0.98	0.97
$q_{LPO,DW}$ [$m^3\,h^{-1}$]	6.1	7.0
$\alpha_{HPO,DW}$ [-]	0.50	0.48
$q_{HPO,DW}$ [$m^3\,h^{-1}$]	0.6	1.0
$\alpha_{in,DO}$ [-]	0.15	0.24
$q_{in,DO}$ [$m^3\,h^{-1}$]	13.9	13.0
FS_{DO} [-]	0.15	0.27
$\alpha_{LPO,DO}$ [-]	0.83	0.82
$q_{LPO,DO}$ [$m^3\,h^{-1}$]	2.0	3.5
$\alpha_{w,Prod}$ [-]	0.03	0.03
$q_{w,Prod}$ [$m^3\,h^{-1}$]	11.9	9.5
$\alpha_{o,Prod}$ [-]	0.94	0.92
$q_{o,Prod}$ [$m^3\,h^{-1}$]	8.1	10.5

Table G.2: Optimal operation for two flow rates when the oil cut in the inlet flow is kept constant at α_{in}=0.4. The estimated flow splits (FS), oil cuts (α) and flow rates (q) for all the streams in the separation system are included.

Variable	q_{in}=20 $m^3\,h^{-1}$	q_{in}=25 $m^3\,h^{-1}$
FS_G [-]	0.33	0.46
α_t [-]	0.94	0.71
q_t [$m^3\,h^{-1}$]	6.7	11.6
α_b [-]	0.13	0.13
q_b [$m^3\,h^{-1}$]	13.3	13.4
FS_{DW} [-]	0.91	0.89
$\alpha_{LPO,DW}$ [-]	0.98	0.75
$q_{LPO,DW}$ [$m^3\,h^{-1}$]	6.1	10.4
$\alpha_{HPO,DW}$ [-]	0.50	0.33
$q_{HPO,DW}$ [$m^3\,h^{-1}$]	0.6	1.2
$\alpha_{in,DO}$ [-]	0.15	0.15
$q_{in,DO}$ [$m^3\,h^{-1}$]	13.9	14.6
FS_{DO} [-]	0.15	0.17
$\alpha_{LPO,DO}$ [-]	0.83	0.75
$q_{LPO,DO}$ [$m^3\,h^{-1}$]	2.0	2.4
$\alpha_{w,Prod}$ [-]	0.03	0.03
$q_{w,Prod}$ [$m^3\,h^{-1}$]	11.9	12.2
$\alpha_{o,Prod}$ [-]	0.94	0.75
$q_{o,Prod}$ [$m^3\,h^{-1}$]	8.1	12.8